



## Spatial distributions of $X_{CO_2}$ seasonal cycle amplitude and phase over northern high latitude regions

Nicole Jacobs<sup>1</sup>, William R. Simpson<sup>1</sup>, Kelly A. Graham<sup>2</sup>, Christopher Holmes<sup>2</sup>, Frank Hase<sup>3</sup>, Thomas Blumenstock<sup>3</sup>, Qiansi Tu<sup>3</sup>, Matthias Frey<sup>3,4</sup>, Manvendra K. Dubey<sup>5</sup>, Harrison A. Parker<sup>5,6</sup>, Debra Wunch<sup>7</sup>, Rigel Kivi<sup>8</sup>, Pauli Heikkinen<sup>8</sup>, Justus Notholt<sup>9</sup>, Christof Petri<sup>9</sup>, and Thorsten Warneke<sup>9</sup>

<sup>1</sup>Department of Chemistry and the Geophysical Institute, University of Alaska Fairbanks, Fairbanks, AK, USA

<sup>2</sup>Department of Earth, Ocean, and Atmospheric Science, Florida State University, Tallahassee, FL, USA

<sup>3</sup>Karlsruhe Institute of Technology (KIT), Institute of Meteorology and Climate Research, Karlsruhe, Germany

<sup>4</sup>National Institute for Environmental Studies, Tsukuba, Japan

<sup>5</sup>Earth and Environmental Sciences, Los Alamos National Laboratory, Los Alamos, NM, USA

<sup>6</sup>California Institute of Technology, Pasadena, CA, USA

<sup>7</sup>Department of Physics, University of Toronto, Toronto, Canada

<sup>8</sup>Finnish Meteorological Institute, Sodankylä, Finland

<sup>9</sup>Institute of Environmental Physics, University of Bremen, Germany

**Correspondence:** William Simpson (wrsimpson@alaska.edu)

**Abstract.** Satellite-based observations of atmospheric carbon dioxide ( $CO_2$ ) provide measurements in remote regions, such as the biologically sensitive but under sampled northern high latitudes, and are progressing toward true global data coverage. Recent improvements in satellite retrievals of total column-averaged dry air mole fractions of  $CO_2$  ( $X_{CO_2}$ ) from the NASA Orbiting Carbon Observatory 2 (OCO-2) have allowed for unprecedented data coverage of northern high latitude regions, while maintaining acceptable accuracy and consistency relative to ground-based observations, and finally providing sufficient data in spring and autumn for analysis of the satellite-observed  $X_{CO_2}$  seasonal cycles across a majority of terrestrial northern high latitude regions. Here, we present an analysis of  $X_{CO_2}$  seasonal cycles calculated from OCO-2 data for temperate, boreal, and tundra regions, subdivided into  $5^\circ$  latitude by  $20^\circ$  longitude zones. We quantify the seasonal cycle amplitudes (SCA) and the annual half drawdown day (HDD). OCO-2 SCA is in good agreement with ground-based observations at five high latitude sites and OCO-2 SCA show very close agreement with SCA calculated for model estimates of  $X_{CO_2}$  from the Copernicus Atmospheric Monitoring Services (CAMS) global inversion-optimized greenhouse gas flux model v19r1. Model estimates of  $X_{CO_2}$  from the GEOS-Chem  $CO_2$  simulation version 12.7.2 with underlying biospheric fluxes from CarbonTracker2019 yield SCA of larger magnitude and spread over a larger range than those from CAMS and OCO-2; however, GEOS-Chem SCA still exhibit a very similar spatial distribution across northern high latitude regions to that from CAMS and OCO-2. Zones in the Asian Boreal Forest were found to have exceptionally large SCA and early HDD, and both OCO-2 data and model estimates yield a distinct longitudinal gradient of increasing SCA from west to east across the Eurasian continent. Longitudinal gradients in both SCA and HDD are at least as pronounced as meridional gradients (with respect to latitude), suggesting an essential role for global atmospheric transport patterns in defining  $X_{CO_2}$  seasonality. GEOS-Chem surface contact tracers show that the largest  $X_{CO_2}$  SCA occurs in areas with the greatest contact with land surfaces, integrated over 15-30 days. The correlation of



$X_{CO_2}$  SCA with these land contact tracers are stronger than the correlation of  $X_{CO_2}$  SCA with the SCA of  $CO_2$  fluxes within each  $5^\circ$  latitude by  $20^\circ$  longitude zone. This indicates that accumulation of terrestrial  $CO_2$  flux during atmospheric transport is a major driver of regional variations in  $X_{CO_2}$  SCA.

## 5 1 Introduction

The changing climate influences carbon exchange in every ecosystem on the planet and polar amplification is driving more rapid changes at higher latitudes (Smith et al., 2019; Park et al., 2018; Pithan and Mauritsen, 2014; Holland and Bitz, 2003; Manabe and Wetherald, 1975). An understanding of the rapidly changing carbon dynamics at high northern latitudes is necessary to improve our understanding of global carbon exchange. However, despite the apparent importance of northern high latitude regions in quantifying the global carbon budget, Bradshaw and Warkentin (2015) point out that a great deal of uncertainty remains in the spatial patterns of carbon stocks and fluxes in Boreal Forest regions, and their results from predictive climate models show that the Boreal Forest may eventually shift from a carbon sink to a carbon source. Euskirchen et al. (2017), Barlow et al. (2015), and Pan et al. (2011) all point out that a shortage of observations in Boreal Forest regions is a major impediment to understanding global carbon uptake, motivating further exploration of alternative data sources, such as satellite measurements. Since pioneering work by Thoning et al. (1989), analysis of the seasonal cycles of atmospheric  $CO_2$  concentrations has been widely used to evaluate carbon exchange dynamics, and the amplitude of the regular seasonal oscillations in atmospheric  $CO_2$  concentrations is a common metric used to infer relative  $CO_2$  uptake. Many studies have combined process-based and atmospheric transport modeling with in situ and airborne observations to infer long-term temporal trends and spatial distributions of seasonal  $CO_2$  exchange, and concluded that Boreal Forest regions play an essential role in global carbon dynamics (Lin et al., 2020; Yin et al., 2018; Piao et al., 2017; Barlow et al., 2015; Bradshaw and Warkentin, 2015; Gauthier et al., 2015; Graven et al., 2013; Pan et al., 2011; Tans et al., 1990). Lin et al. (2020) compared seasonal cycle amplitudes (SCA) from surface in situ measurements of  $CO_2$  to those estimated from GEOS-Chem transport modeling coupled with CAMS v17r1 flux estimates, and found that Siberia had the largest SCA of any region considered when normalized for area. Furthermore, Lin et al. (2020) found that even though Siberia is a relatively small source region, fluxes from Siberia were the second most influential in determining SCA of in situ  $CO_2$  on a global scale, following those from Northern Hemisphere midlatitudes.

It has been well established that the SCA of atmospheric  $CO_2$  increases with latitude in the Northern Hemisphere due to the increased seasonal attenuation of sunlight which drives more extreme seasonality in temperature and ecosystem productivity at higher latitudes. There is general consensus that this meridional gradient in SCA is increasing over time, so that while  $CO_2$  SCA are increasing across the Northern Hemisphere, the SCA at higher northern latitudes are increasing at an accelerated rate. There is still some controversy regarding what mechanisms are driving changes in  $CO_2$  SCA and how spatial distributions or



temporal trends in CO<sub>2</sub> seasonality are influenced by atmospheric transport patterns or regional changes in carbon exchange. Recent work by Liu et al. (2020) suggests that global increases in CO<sub>2</sub> SCA since the 1960's are a result of increases in growing season mean temperatures, and polar amplified warming would then explain the increase in the meridional gradients in SCA. Studies by Piao et al. (2017), Forkel et al. (2016), and Graven et al. (2013) used global models to show that increasing meridional gradients in SCA are driven by the ecological effects of climate change and changes in vegetation, primarily suggesting CO<sub>2</sub> fertilization as the dominant mechanism. This point is confirmed by findings from Bastos et al. (2019) that attribute enhanced SCA in Boreal Asia and Europe to increases in net biome productivity as a result of CO<sub>2</sub> fertilization. Although they do not address the increase in meridional gradients over time, Zeng et al. (2014) and Gray et al. (2014) argue that agricultural expansion in the Northern Hemisphere midlatitudes has resulted in increases in seasonal carbon exchange, which, in turn, result in larger SCA of CO<sub>2</sub> concentrations on a global scale. Barnes et al. (2016) suggest that it is actually the Temperate Forest between 30°N and 50°N that is the dominant driver of seasonal carbon exchange on global scales. Yet another study by Yin et al. (2018) found evidence that challenged previous assumptions about the relationship between seasonal cycle amplitude and spring and autumn temperatures in northern high latitudes, emphasizing the need for continued data-driven model validation for these regions. Despite their disagreements, most agree that the seasonality in atmospheric CO<sub>2</sub> at northern high latitudes, and specifically the Boreal Forest, require continued attention as carbon dynamics continue to change. While this paper does not consider temporal changes in SCA, an assessment of spatial distributions of SCA implied by satellite-based observations over northern high latitude terrestrial regions can provide a good foundation for exploring temporal changes in these spatial distributions in later analyses.

Satellite-based infrared spectrometers like the NASA Orbiting Carbon Observatory 2 (OCO-2) (O'Dell et al., 2018; Wunch et al., 2017; Crisp et al., 2017), SCIAMACHY (Reuter et al., 2011; Bovensmann et al., 1999; Burrows et al., 1995), and GOSAT (Basu et al., 2013; Yoshida et al., 2013; Hamazaki et al., 2005) provide global measurements of column-averaged dry air mole fractions of CO<sub>2</sub> ( $X_{CO_2}$ ), and particularly can quantify  $X_{CO_2}$  in remote, un-instrumented regions. Retrievals and instrument technologies have been advancing rapidly, and boreal-forest-specific methods of  $X_{CO_2}$  bias correction and quality control filtering have been developed and validated where ground truth exists (Jacobs et al., 2020b; Kiel et al., 2019; O'Dell et al., 2018). In addition, the development of collaborative networks of ground-based solar-viewing spectrometers, including the Total Carbon Column Observing Network (TCCON) and the Collaborative Carbon Column Observing Network (COCCON), has provided a framework for robust global validation of similar passive satellite-based observations (Frey et al., 2019; Wunch et al., 2011). These combined efforts of satellite-based and ground-based total atmospheric column measurements of CO<sub>2</sub> offer a wealth of opportunities for gaining insights into the global climate system as a whole.

In this manuscript, we quantify and analyze seasonal cycle parameters derived directly from satellite-based observations of  $X_{CO_2}$ , across the northern high latitude terrestrial regions. This work represents progress in the application of global monitoring of atmospheric CO<sub>2</sub> to the continued evaluation of global scale carbon dynamics, and shows how satellites like OCO-2 can be used to monitor CO<sub>2</sub> biospheric exchange. In this analysis, OCO-2 data over terrestrial northern high latitudes is used to explore spatial distributions of seasonal cycle amplitude (SCA) and seasonal cycle phase. Interpretation of these spatial distributions can be used to test previous claims and provide new insights into what is driving carbon exchange at northern



high latitudes. In particular, we explore how seasonality in  $X_{CO_2}$  differs for the North American, European, and Asian Boreal Forest regions, and how the Boreal Forest fits within the broader context of northern high latitude regions. In addition, seasonal cycle parameters derived from OCO-2 observations are combined with those from ground-based TCCON and COCCON observations, then compared with seasonal cycle parameters from two model frameworks: the Copernicus Atmospheric Monitoring Services (CAMS) global inversion-optimized greenhouse gas flux model estimates of  $X_{CO_2}$  (Chevallier, 2020b), with in situ data assimilation, and the GEOS-Chem  $CO_2$  simulation (Nassar et al., 2010) with underlying biosphere fluxes from CarbonTracker2019 (Jacobson et al., 2020). Ultimately, we use the GEOS-Chem  $CO_2$  simulation to address the question of how much spatial variability in  $X_{CO_2}$  seasonal cycle parameters may be attributed to magnitudes of fluxes within the observation zones and how much may be attributed to the regional and continental scale accumulation of  $CO_2$  fluxes during atmospheric transport.

## 2 Methods

### 2.1 OCO-2 data

The NASA Orbiting Carbon Observatory 2 (OCO-2) launched in 2014 and began collecting data in September of that year. Daily averages of  $X_{CO_2}$  are calculated for each zone using observations from OCO-2 B9 Lite files (OCO-2 Science Team/Michael Gunson, Annmarie Eldering, 2018). Ongoing improvements in the ACOS retrieval algorithm and previous efforts by Jacobs et al. (2020b) to develop quality control thresholds tailored to OCO-2 B9 retrievals over Boreal Forest regions (Boreal QC) have allowed sufficient data over our  $5^\circ$  latitude by  $20^\circ$  longitude zones to construct  $X_{CO_2}$  time-series that yield robust seasonal cycle parameterization. The Boreal QC was evaluated for use with terrestrial OCO-2 B9 retrievals north of  $50^\circ N$  (Jacobs et al., 2020b), and the zones considered here cover the majority of land north of  $50^\circ N$ . The southern boundaries of the southern-most zones of North America are at  $47^\circ N$ , but the  $3^\circ$  of latitude is not expected to significantly impact the effectiveness of the Boreal QC filtering. Instead of the standard B9 bias correction, we use a modified bias correction that includes temperature at 700 hPa (T700), as discussed by Jacobs et al. (2020b), because it was found in previous results to reduce the seasonality of OCO-2 bias relative to ground-based TCCON and EM27/SUN measurements. Seasonal cycle fits to OCO-2 retrievals of  $X_{CO_2}$  with the standard global B9 bias correction were also calculated and compared to model-derived seasonal cycle fits in the supplement (see Sect. S2).

### 2.2 TCCON and EM27/SUN data

The Total Carbon Column Observing Network (TCCON) is a ground-based network of sites observing  $X_{CO_2}$  using high spectral resolution solar-viewing Fourier transform infrared spectrometers (FTS). Data are included from four TCCON sites: East Trout Lake, Canada in North American Boreal zone 3 (Wunch et al., 2018); Sodankylä, Finland in European Boreal zone 6 (Kivi et al., 2014; Kivi and Heikkinen, 2016); Białystok, Poland in European Temperate zone 2 (Deutscher et al., 2019); Bremen, Germany in European Temperate zone 3 (Notholt et al., 2019) (see site details in Table 1 and locations mapped in Fig. 1).





**Table 1.** Summary of instrument type, years of observations, geographic coordinates, and corresponding coordinates of the nearest model grid point in CAMS and GEOS-Chem (GC) for each ground site.

Site	Type	Years	latitude	longitude	CAMS latitude	CAMS longitude	GC latitude	GC longitude
Bialystok	TCCON	2014-2018	53.23°N	23.03°E	54.0°N	22.5°E	54.0°N	22.5°E
Bremen	TCCON	2014-2019	53.1°N	8.85°E	54.0°N	7.5°E	54.0°N	10.0°E
East Trout Lake	TCCON	2016-2019	54.35°N	104.99°W	54.0°N	105.0°W	54.0°N	105.0°W
Sodankylä	TCCON	2014-2019	67.26°N	26.25°E	67.37°N	26.63°E	68.0°N	27.5°E
Fairbanks	EM27/SUN	2016-2019	64.86°N	147.85°W	65.37°N	146.25°W	64.0°N	147.5°W

The Collaborative Carbon Column Observing Network (COCCON) is a network of sites observing with the Bruker EM27/SUN FTS (Gisi et al., 2012), which are lower resolution mobile solar-viewing spectrometers that serve as complement to TCCON measurements. EM27/SUN observations have been compared to TCCON observations in multiple studies, most notably Sha et al. (2020), Tu et al. (2020), Frey et al. (2019), Velazco et al. (2018), and Hedelius et al. (2017). In most of these comparisons EM27/SUN and TCCON observations agree with biases less than 0.25 ppm on average. In some cases offsets between EM27/SUN and TCCON observations are reported to be as large as 2 ppm, but the proven stability of the EM27/SUN should allow for a bias correction that would yield good agreement between TCCON and EM27/SUN retrievals. The EM27/SUN instruments have measured  $X_{CO_2}$  in a number of campaigns to validate OCO-2 and other satellite-based observations, including work by Jacobs et al. (2020b), Velazco et al. (2018), and Klappenbach et al. (2015), suggesting good agreement between EM27/SUN observations and satellite-based observations. In this analysis, observations with an EM27/SUN FTS in Fairbanks, Alaska, USA (65.859°N, 147.850°W; Jacobs et al. (2020a)) are used as a fifth ground-based comparison in the Boreal Forest. Fairbanks is an established COCCON site as of 2018, so the instrument participates regularly in performance and calibration checks at the central facility operated by KIT and data processed in compliance with COCCON recommendations are available. In this study, we use the GGG2014 retrieval algorithm coupled with the EM27/SUN GGG interferogram processing suite (EGI; Hedelius and Wennberg (2017)) instead of the standard COCCON retrieval methods for consistency with TCCON retrievals and because this data product has already been bias corrected to TCCON using side-by-side observations at Caltech, as described in detail by Jacobs et al. (2020b). Seasonal cycle fits for ground-based observations at these five sites use daily averages of retrievals collected within two hours of local solar noon, weighted by retrieval error, as described by Jacobs et al. (2020b). We refer to these daily averages as near noon ground-based (NNG) observations.

### 2.3 CAMS model estimates

Model estimates of  $X_{CO_2}$  from the Copernicus Atmospheric Monitoring Services (CAMS) global inversion-optimized greenhouse gas flux model v19r1 are used here as a model comparison to OCO-2 and NNG data. The modeling framework for CAMS  $CO_2$  flux inversions is described in detail by Chevallier (2020b). Quality assessments for the Northern Hemisphere by Chevallier (2020a) report that nearly all biases in both CAMS estimates of in situ  $CO_2$  relative to unassimilated aircraft



observations and CAMS estimates of  $X_{CO_2}$  relative to TCCON observations are within 1 ppm, with standard deviation in bias around 2 ppm. CAMS estimates of  $X_{CO_2}$  are available as daily averages and have  $1.9^\circ$  latitude by  $3.75^\circ$  longitude spatial resolution, which is sufficient for providing multiple grid-points within each zone and coincidence with most ground sites within approximately 100 km (see Table S1 in the supplement for exact coordinates of grid-points nearest to the ground sites).

- 5 We use CAMS model estimates with data assimilation from a global network of surface in situ observations at 119 locations, but without any satellite data assimilation. In addition to the  $X_{CO_2}$  estimates, the CAMS model output includes surface flux estimates, which will be considered further in the Discussion, Sect. 4.3. Both CAMS flux estimates and CAMS  $X_{CO_2}$  estimates use the same atmospheric transport modeling framework.

#### 2.4 GEOS-Chem $CO_2$ and Transport Tracer simulations with CarbonTracker2019 land and ocean fluxes

- 10 The GEOS-Chem atmospheric transport model version 12.7.2 (more detailed information at [www.geoschem.org](http://www.geoschem.org)) has  $2^\circ$  latitude by  $2.5^\circ$  longitude spatial resolution, using MERRA-2 meteorology (Gelaro et al., 2017). We use the GEOS-Chem  $CO_2$  simulation (Nassar et al., 2010) and GEOS-Chem surface contact tracers, for 2014-2016, to examine the relationships between seasonal cycle parameters and atmospheric transport patterns and speculate on the role of atmospheric transport in determining spatial distributions of  $X_{CO_2}$  seasonality across northern high latitudes. The GEOS-Chem  $CO_2$  simulation provides daily
- 15  $X_{CO_2}$  estimates and source attribution with underlying fluxes from the NOAA Earth Systems Research CarbonTracker2019 (Jacobson et al., 2020) for land and ocean biospheric exchange, the Community Emissions Data System (CEDS; Hoesly et al., 2018) for fossil fuel emissions, the Global Fire Emissions Database, Version 4.1 (GFED4.1s; Randerson et al., 2018; van der Werf et al., 2017) for biomass burning emissions, and results from Bukosa (2019) for the chemical production of  $CO_2$  in the atmosphere. For the fossil fuel emissions, the CEDS inventory ended in 2014, so 2015 and 2016 emissions were scaled by
- 20 the CEDS 2014 emissions to match the global total in those later years, as reported by the Open-Source Data Inventory for Anthropogenic Carbon Dioxide (ODIAC; Oda and Maksyutov, 2011). We used this approach, rather than using ODIAC alone, because the CEDS inventory includes anthropogenic biofuel emissions that are not in ODIAC.  $CO_2$  from each source type is tagged within the model to quantify their contributions to total column  $CO_2$ . Unlike the CAMS model, which has optimized  $CO_2$  flux and  $X_{CO_2}$  estimates with the same atmospheric transport model, CarbonTracker2019 fluxes are estimated using
- 25 TM5 to simulate atmospheric transport rather than the GEOS-Chem transport model, while the fossil fuel and biomass burning flux estimates used in the GEOS-Chem  $CO_2$  simulation are based on inventory estimates that may involve other assumptions about atmospheric transport. The GEOS-Chem surface contact tracer simulations include tracers emitted uniformly from land or ocean, which subsequently decay with e-fold lifetimes of 5, 15, 30, or 90 days. These surface contact tracers are used to evaluate how  $X_{CO_2}$  SCA is influenced by transport from upwind land or ocean surfaces on various timescales. GEOS-Chem
- 30 simulations are run for 2014-2016 rather than for the precise OCO-2 data period, but analysis shown in the supplement (see Sect. S2) demonstrates that SCA and HDD are mostly unchanged when calculated for 2014-2016 instead of 2014-2019.



## 2.5 Regions and zones

We define regions in North America, Europe, and Asia, which are further subdivided into 5° latitude by 20° longitude zones, and zones are designated as temperate, boreal, or tundra. For the purposes of this analysis, the classification of zones as temperate, boreal, or tundra, as well as the longitudinal division between the European and Asian regions are guided by maps of ecoregions from Hayes et al. (2011) and Euskirchen et al. (2007) (see Fig. 1). The Boreal Forest zones considered cover a narrower range of latitudes than the boreal regions defined for the Transcom 3 ecoregions (Gurney et al., 2000), which include all high Arctic tundra and portions of temperate Asia as part of the boreal regions. Otherwise, the North American Boreal region and Eurasian Boreal region defined by Transcom 3 are very similar to the North American Boreal and Asian Boreal regions defined in this analysis. We differ markedly from Transcom 3 in defining separate European Boreal and European Temperate regions, while Transcom 3 combines all of Europe into a single European region. In North America, the zones are shifted by 3° latitude relative to the zones in Eurasia; starting at 47°N and extending in to 72°N in 5° increments. This was done to bring ground sites in the North American Boreal region closer to the center latitude of their encompassing zones and to more accurately fit the boundaries of temperate, boreal, and tundra biomes.

Also shown in Fig. 1 are the locations of five ground sites where long-term observations of  $X_{CO_2}$  have been collected (see Table 1 for details). These ground sites include two sites in the European Temperate region (Białystok and Bremen), one site in the European Boreal region (Sodankylä), and two sites in the North American Boreal region (East Trout Lake and Fairbanks). Ground-based data are explained further in Sect. 2.2 and seasonal cycles of ground-based data are compared to satellite and model-derived seasonal cycles in Sect. 3.1.

## 2.6 $X_{CO_2}$ seasonal cycle modeling and parameters

The primary focus of our analysis is characterizing seasonality in  $X_{CO_2}$  and exploring how and why this seasonality differs across regions of the Boreal Forest. To this end, time-series are constructed using daily average  $X_{CO_2}$  from satellite retrievals, ground-based solar-viewing FTIR spectrometers, and CAMS model estimates with data assimilation from in situ surface concentrations. Seasonal cycles are characterized following methods used by Lindqvist et al. (2015), in which daily mean  $X_{CO_2}$  are fit to a skewed sine wave of the form

$$f(t) = a_0 + a_1 t + a_2 \sin(\omega[t - a_3] + \cos^{-1}[a_4 \cos(\omega[t - a_5])]) \quad (1)$$

where  $t$  is days,  $\omega = \frac{2\pi}{365.25}$ , the interannual trend is defined by  $a_0 + a_1 t$ , and the seasonal cycle amplitude (SCA) is defined by  $2|a_2|$ . The fit is calculated using nonlinear least squares optimization with standard error defined as the mean daily standard deviations in retrieved  $X_{CO_2}$ . As a metric for seasonal timing we define half drawdown day (HDD) as the day of year when the detrended seasonal cycle fit,  $f(t) - a_0 - a_1 t$ , crosses zero from positive to negative.

The approach used by Lindqvist et al. (2015) was found to be more numerically stable than fitting to a truncated Fourier Series, as has been employed in previous studies (Wunch et al., 2013; Thoning et al., 1989), because periods of missing data can produce unrealistic oscillations in a Fourier series fit. Even for zones with the longest winter gaps in observations, the shape of the seasonal cycle fit using Eq. 1 only has one annual maximum and minimum.



### 3 Results

#### 3.1 $X_{CO_2}$ seasonal cycles near ground sites

Before attempting to interpret spatial distributions of seasonal cycle parameters on continental scales, it is of value to get a better idea of how seasonal cycle parameters from observations at a single location compare to those from spatially averaged data. To this end, five high latitude sites are considered with long term ground-based observations, as described in Sect. 2.2, and seasonal cycle fits to near noon ground-based (NNG) observations at these sites are compared to those from spatially averaged data over a commonly used satellite coincidence region of  $5^\circ$  latitude by  $10^\circ$  longitude centered on the location of the ground site, as well as over the  $5^\circ$  latitude by  $20^\circ$  longitude zone in which the ground site is located (reference zones in Fig. 1). In Fig. 2, observed SCA and HDD from NNG and OCO-2 are correlated against model-derived SCA and HDD from CAMS and GEOS-Chem at each of the three spatial scales, and the corresponding linear regression equations and correlation coefficients are reported in Table 2. These correlations exhibit tight linearity for SCA and reasonable linearity for HDD when comparing observed and model-derived parameters at all scales. SCA and HDD from CAMS are in better agreement with observations than those from GEOS-Chem in every case, as demonstrated by the fact that the CAMS linear regression falls closer to the  $y = x$  line in every panel of Fig. 2. Both CAMS and GEOS-Chem tend to yield larger SCA and later HDD than observations, for all three spatial scales, which stands in contrast to earlier work by Yang et al. (2007) who found that the Transcom model underestimated SCA of  $CO_2$  mixing ratios relative to aircraft observations at nearly every altitude. Details of the full time-series, plots of seasonal cycle fits, and seasonal cycle fit parameters for these ground sites, coincidence regions, and encompassing zones are reported in Sect. S1.1 of the supplement.

In Fig. 3 and Table 3 the relationships between seasonal cycle parameters from a single point, at or nearest the ground sites, and spatially averaged data are explored, in this case NNG are correlated against spatially averaged OCO-2 retrievals, while model estimates near the ground site are correlated against spatially averaged model estimates. Jacobs et al. (2020b) have shown that an alternative bias correction, parameterized for temperature at 700 hPa, resulted in reduced seasonality in OCO-2 bias within the  $5^\circ$  latitude by  $10^\circ$  longitude coincidence region relative to NNG observations at East Trout Lake, Sodankylä, and Fairbanks. Results in the supplement show that the alternative bias correction improved agreement in both SCA and HDD between NNG seasonal cycles and coincident OCO-2 seasonal cycles. The results in Fig. 3 and Table 3 indicate that HDD correlations across scales tend to be slightly weaker and markedly different depending on whether one considers observed or model-derived seasonal cycles. For the coincidence region and the encompassing zone, OCO-2 data consistently yield later HDD than NNG, while spatially averaged model estimates tend to yield HDD that is in good agreement or slightly earlier than the point nearest to the ground site. SCA for ground sites are well correlated and mostly in close agreement with both SCA for  $5^\circ$  latitude by  $10^\circ$  longitude coincidence regions and SCA for encompassing  $5^\circ$  latitude by  $20^\circ$  longitude zones. The relatively weaker correlations in HDD across spatial scales suggest greater spatial heterogeneity in HDD within zones from both observed and model-derived seasonal cycles, while SCA appears to scale well with spatial averaging.



**Table 2.** Linear regression equations and correlation coefficients for the correlations in Fig. 2 comparing model-derived and observed SCA and HDD at different scales for five ground sites.

Panel	CAMS fit	CAMS R <sup>2</sup>	GEOS-Chem fit	GEOS-Chem R <sup>2</sup>
(a)	$y = 0.84x + 1.92$	0.840	$y = 0.90x + 1.98$	0.872
(b)	$y = 0.84x + 1.94$	0.657	$y = 1.04x + 0.87$	0.754
(c)	$y = 0.89x + 1.31$	0.797	$y = 1.03x + 0.91$	0.834
(d)	$y = 0.79x + 38.65$	0.585	$y = 0.47x + 98.21$	0.622
(e)	$y = 0.44x + 95.62$	0.470	$y = 0.35x + 117.36$	0.432
(f)	$y = 0.66x + 56.85$	0.515	$y = 0.48x + 94.97$	0.385

**Table 3.** Linear regression equations and correlation coefficients for the correlations in Fig. 3 in which SCA and HDD from NNG or model estimates near the ground sites are compared to SCA and HDD from spatially averaged satellite observations or spatially averaged model estimates over the corresponding 5° latitude by 10° longitude coincidence regions and encompassing 5° latitude by 20° longitude zones.

Panel	observed fit	observed R <sup>2</sup>	CAMS fit	CAMS R <sup>2</sup>	GEOS-Chem fit	GEOS-Chem R <sup>2</sup>
(a)	$y = 0.82x + 1.44$	0.808	$y = 1.03x - 0.47$	0.986	$y = 1.13x - 1.38$	0.984
(b)	$y = 0.92x + 0.71$	0.889	$y = 1.04x - 0.55$	0.958	$y = 1.12x - 1.21$	0.974
(c)	$y = 1.38x - 60.07$	0.666	$y = 0.99x + 1.00$	0.892	$y = 1.50x - 89.00$	1.000
(d)	$y = 1.29x - 45.32$	0.698	$y = 1.26x - 46.00$	0.839	$y = 1.94x - 167.50$	0.958

### 3.2 $X_{CO_2}$ seasonal cycles by zone

The full set of seasonal cycle fit parameters and their standard errors for each zone and ground site in Fig. 1 are reported in the supplement for OCO-2 data, NNG data, CAMS model estimates, and GEOS-Chem model estimates. Time-series of daily averages with daily standard deviations, the seasonal cycle fits, and fit residuals for OCO-2 observations are plotted in Figures S4 through S11. Time-series of daily model estimates, the model-derived seasonal cycle fits, and the corresponding OCO-2 seasonal cycle fits are plotted in the Figures S13 through S28. While the fits to model estimates are generally similar in shape with fits to observations, there are some zones that yield an unrealistic drop in wintertime values in the OCO-2 seasonal cycle fits, which is more pronounced for zones with fewer satellite-based  $X_{CO_2}$  observation near the peak and trough of the seasonal cycle. This wintertime drop in the shape of the seasonal cycle is evidence that should motivate further efforts to increase satellite-based observations over high latitude regions outside of the summer months. Only a small number of zones, particularly the two most northern Asian Tundra zones, are obviously compromised by insufficient data in spring and autumn, most of the zones that exhibit a wintertime drop in the seasonal cycle fit still yield SCA that are comparable to corresponding results from CAMS and GEOS-Chem. The close similarities between spatial distributions of seasonal cycle parameters from OCO-2, CAMS, and GEOS-Chem are apparent in Fig. 4. Direct correlations between observational and model-derived SCA



and HDD are included in the supplement (see Fig. S29) in which GEOS-Chem was found to have correlation coefficients of 0.738 and 0.449, and CAMS was found to have correlation coefficients of 0.644 and 0.556, for SCA and HDD respectively. The most notable discrepancies in SCA between OCO-2 and CAMS occur in the Asian and North American tundra regions for which CAMS estimates yield larger and more homogeneous values of SCA than OCO-2 data; however, some of the OCO-2 seasonal cycle fits for the Tundra zones are compromised by insufficient data coverage. Overall, model estimates tend to yield larger SCA and later HDD than OCO-2 and NNG. Even though SCA and HDD derived from GEOS-Chem cover a broader range of values, particularly over-estimating SCA in the Asian Boreal and Tundra regions and predicting later HDD in a number of Temperate and Boreal zones, GEOS-Chem seasonal cycles remain strongly correlated with observed seasonal cycles. Results in the supplement (see Fig. S30) indicate that SCA derived from clipped time-series of OCO-2 and CAMS (restricted to 2014-2016) were only marginally different from SCA derived for the full time (2014-2019), suggesting that the different results in GEOS-Chem are not likely to be caused by the shorter duration of model output.

### 3.3 Spatial distributions of SCA and HDD

Seasonal cycle amplitudes (SCA) and half drawdown day (HDD) are mapped in Fig. 4, showing results from OCO-2 observations, CAMS model estimates, and GEOS-Chem model estimates. Figure 4 demonstrates that both OCO-2 observations and model estimates from CAMS and GEOS-Chem yield larger SCA and earlier HDD in the Asian Boreal Forest than any other region. The earlier seasonal timing of the Asian Boreal Forest zones is consistent with results from Keppel-Aleks et al. (2012) and Schneising et al. (2011), and these studies also linked earlier drawdown in Asia to larger SCA. Although one would not necessarily expect SCA of surface in situ measurements to match SCA of  $X_{CO_2}$ , this finding also aligns with the study by Lin et al. (2020), who found that Siberia had the largest SCA in surface  $CO_2$  concentrations when normalized for area. The CAMS and GEOS-Chem results in Fig. 4 follow a much more systematic distribution with pronounced meridional gradients, whereas the results from OCO-2 show more spatial heterogeneity, and this is particularly true for HDD. Seasonal cycles of direct observations are expected to display more heterogeneity than seasonal cycles of model estimates, which depend on mathematical modeling of atmospheric transport to calculate  $X_{CO_2}$ , even if the underlying fluxes are based on in situ data assimilation. Overall, the spatial distributions in SCA and HDD from OCO-2 agree more with those from CAMS than from GEOS-Chem estimates, which produce larger magnitudes of SCA for many regions, as well as SCA and HDD spread across a larger range. In addition, OCO-2 observations yield notably smaller SCA than CAMS or GEOS-Chem in the western zones of the Asian Boreal Forest, in the Asian Tundra, and in the eastern zones of North America.

Figure 5, panels (b), (d), and (f) show a clear increase in SCA from west to east across the Eurasian continent in both model-derived and observational results. In North America, longitudinal gradients are more subtle. While OCO-2 observations exhibit a slight gradient across North America that increases east to west, CAMS and GEOS-Chem yield SCA that increase from west to east, remaining consistent with gradients for Eurasia. This discrepancy in North America hinges primarily on the zones of Boreal Forest and Tundra in eastern North America, which have the smallest SCA for that continent when using OCO-2 data, but have the largest SCA for that continent when using CAMS or GEOS-Chem model estimates. As expected, panels (a), (c), and (e) of Fig. 5 show a meridional gradient with increasing SCA from south to north for both observational





**Table 4.** Linear regression equations and correlation coefficients for the correlations in Fig. 7 in which SCA is correlated against HDD for observed and model-derived results. Linear regressions were calculated considering all 5° latitude by 20° longitude zones, and then separately for zones in temperate, boreal, and tundra regions.

Ecoregion(s)	observed fit	observed R <sup>2</sup>	CAMS fit	CAMS R <sup>2</sup>	GEOS-Chem fit	GEOS-Chem R <sup>2</sup>
All	$y = -0.10x + 27.48$	0.182	$y = -0.06x + 21.82$	0.066	$y = -0.17x + 42.06$	0.346
Temperate	$y = -0.10x + 27.01$	0.151	$y = -0.11x + 27.87$	0.311	$y = -0.15x + 37.05$	0.606
Boreal	$y = -0.18x + 41.54$	0.514	$y = -0.18x + 42.30$	0.596	$y = -0.24x + 54.27$	0.843
Tundra	$y = -0.21x + 47.45$	0.744	$y = -0.13x + 34.88$	0.617	$y = -0.20x + 47.55$	0.823

and model-derived seasonal cycles. However, the Asian Boreal Forest zones stand apart from other regions in all panels of Fig. 5, particularly when plotted against latitude, with larger SCA than other data at similar latitude or longitude. Results in Fig. 6 demonstrate that HDD are far more scattered and do not follow the distinct trends with latitude and longitude that SCA does. HDD spatial gradients seem to be inverted relative to SCA with a vague tendency toward later HDD at more northern latitudes and more western longitudes (with similar discrepancies between observed and model-derived longitudinal gradients for North America).

### 3.4 The relationship between SCA and HDD

Figure 7 and the calculated linear regressions in Table 4 show that there is a negative correlation between HDD and SCA for both observed and model-derived seasonal cycle fits, such that earlier HDD corresponds to larger SCA. CAMS model estimates yield correlations between HDD and SCA that are more similar to those from OCO-2 and NNG measurements, while GEOS-Chem yields stronger correlations with steeper slopes. The results in Fig. 7 emphasize the exceptionally early HDD and large SCA of the Asian Boreal Forest, such that many of the Asian Boreal zones fall more in line with the tundra zones than with the other boreal zones. A meridional gradient is suggested by the fact that the linear regressions plotted in Fig. 7 are shifted up for the tundra zones and shifted down for the temperate zones, with the boreal zones in between the two. Furthermore, the separate linear regressions for the temperate, boreal, and tundra zones plotted in Fig. 7 have much larger R<sup>2</sup> than the linear regressions for all the zones together (see Table 4), suggesting that there are different dynamics in different biomes that affect relationships between extent and timing of apparent CO<sub>2</sub> uptake. The strength of this correlation in observed and CAMS seasonal cycles was highest for tundra, and lowest for temperate zones with the boreal zones falling in between.

## 4 Discussion

In this analysis, methods described by Lindqvist et al. (2015) were used to fit daily average time-series of daily  $X_{CO_2}$  to a skewed sine wave (see Eq. 1) and subsequently calculate seasonal cycle amplitude (SCA) and half drawdown day (HDD), as described in Sect. 2.6. These fitting methods have been found to yield more stable and realistic fits for time-series with winter



gaps than fitting to a truncated Fourier Series. Increased OCO-2 throughput (Kiel et al., 2019; O'Dell et al., 2018; Osterman et al., 2018) and use of a bias correction and quality control methods tailored to northern high latitudes (Jacobs et al., 2020b) improve the availability of OCO-2 data at the edges of the growing season and assist in generating stable and realistic seasonal cycle fits. Results in Fig. 3 and Table 3 indicate close agreement between SCA from NNG observations at five ground sites and corresponding SCA from OCO-2 data in the 5° latitude by 10° longitude spatial coincidence regions. Relatively weak correlations in HDD at the five ground sites, both across spatial scales and between observed and model-derived seasonal cycles, are likely to be at least partly attributable to spatial heterogeneity in seasonal cycle timing within 5° latitude by 20° longitude zones. It is possible that HDD as a phase metric is not as well constrained by the seasonal cycle fitting methods used here as SCA. Many of the greatest discrepancies in HDD when comparing coincidence regions or zones to ground sites (see Fig. 3 and Table 3) occur in observed seasonal cycles and may arise from disagreement between NNG and OCO-2 observations. Discrepancies between observed and model-derived HDD, which are most apparent for GEOS-Chem  $X_{CO_2}$  estimates, could reflect an inaccurate representation of ecosystem respiration in the CASA terrestrial biosphere model, which underlies the CarbonTracker2019 biospheric fluxes used in the GEOS-Chem  $CO_2$  simulation. Byrne et al. (2018) found that differences in the seasonal timing of NEE maximum drawdown were primarily driven by differences in the timing of ecosystem respiration in spring and fall, while the amplitude of NEE was largely influenced by the magnitude of peak gross primary production (GPP). This could explain the higher degree of spatial heterogeneity in seasonal cycle timing because ecosystem respiration is driven by soil temperature, soil moisture, and litter accumulation, which could all be expected to exhibit a higher degree of spatially heterogeneity than ambient temperature and sunlight. If there is, in truth, more spatial heterogeneity in the timing of seasonal  $CO_2$  uptake, then a failure to accurately represent these spatial distributions in timing could be exacerbated by errors or differences in atmospheric transport modeling and result in larger or more variable discrepancies between observed and model-derived HDD. In this case, the relatively spatially homogeneous values of SCA would be easier to accurately predict in the models than HDD. Alternatively, if SCA is primarily defined by the magnitude of maximum GPP, it may be better constrained in the models because data products like SIF and NDVI can be used to validate model estimates of GPP, while ecosystem respiration does not have a direct data proxy.

OCO-2, CAMS, and GEOS-Chem all yield very similar spatial distributions of SCA and HDD across the northern high latitude regions (see map in Fig. 1), and both had large SCA and early HDD in the Asian Boreal Forest as well as a clear increase in SCA from west to east across the Eurasian continent. Discrepancies between GEOS-Chem SCA and SCA from both CAMS and observations are consistent with the assessments of seasonal bias resulting from the GEOS-Chem transport modeling framework with MERRA-2 meteorology, as described by Schuh et al. (2019). They found that the GEOS-Chem  $CO_2$  simulation overestimates  $X_{CO_2}$  in winter and underestimates  $X_{CO_2}$  in summer relative to the TM5 transport model, yielding an exaggerated seasonal oscillation and larger SCA. Byrne et al. (2018) found that CarbonTracker2016, using CASA to constrain biospheric carbon exchange, estimated later NEE drawdown than flux inversions with either GOSAT or TCCON data assimilation, and this appears to be consistent with the later HDD estimated by the GEOS-Chem  $CO_2$  simulation. Despite these discrepancies, we contend that the strong correlations between GEOS-Chem and observational results (see Sect. S2 in



the supplement) suggest that GEOS-Chem simulations remain a useful tool for investigating the broader implications of spatial distributions in SCA and HDD from OCO-2 observations.

Two limiting hypotheses for the origin of the spatial patterns in  $X_{CO_2}$  SCA shown in Fig. 4 are that they arise from differences in flux magnitudes within the  $5^\circ$  latitude by  $20^\circ$  longitude zone or that they arise from transport patterns accumulating CO<sub>2</sub> exchanges across multiple zones or regions. To investigate the relative influences of atmospheric transport or fluxes within zones on  $X_{CO_2}$  seasonal cycles, we consider source apportionment from the GEOS-Chem CO<sub>2</sub> simulation (Nassar et al., 2010) and GEOS-Chem surface contact tracers, as well as surface CO<sub>2</sub> flux estimates used in the GEOS-Chem and CAMS models.

#### 4.1 CO<sub>2</sub> source contributions

Through analysis of  $X_{CO_2}$  source attribution in the GEOS-Chem CO<sub>2</sub> simulation, we found that the seasonal variability in  $X_{CO_2}$  for northern high latitudes is overwhelmingly dominated by seasonality in the contribution of terrestrial NEE. Detrended seasonal cycles of all CO<sub>2</sub> sources in GEOS-Chem, averaged by region and day of year, are shown in Fig. 8, demonstrating that the seasonal variability in fossil fuel, fire, and ocean source contributions are negligibly small compared to the seasonal variability in the terrestrial NEE contribution. Furthermore, seasonal cycle fits of GEOS-Chem daily average terrestrial NEE contribution within each zone to Eq. 1 yield SCA and HDD that are very strongly correlated to SCA and HDD from GEOS-Chem  $X_{CO_2}$  (see Fig. 9). Figure 9 also shows that SCA is slightly larger and HDD is slightly earlier for seasonal cycle fits of the terrestrial NEE contribution than for seasonal cycle fits of  $X_{CO_2}$ . Although some zones have large anthropogenic CO<sub>2</sub> sources, these sources are not very seasonal, so do not contribute directly to SCA.

#### 4.2 The role of transport inferred from GEOS-Chem tracers

GEOS-Chem surface contact tracers were used to simulate the release of tracers from land and ocean yielding relative concentrations of tracers with lifetimes of 5, 15, 30, and 90 days for a given grid point and day. The surface contact tracers for a given zone were found to vary minimally in time, so a total average was taken by averaging spatially and temporally within each zone (see map in Fig. 1) and over all days in 2014-2016.

The surface contact tracers show that the largest  $X_{CO_2}$  SCA occurs in areas with the greatest influence from air that contacted land surfaces 15 to 30 days prior. There are clear similarities in the spatial distributions of SCA in panels (a), (c), and (e) of Fig. 4 and those of the surface contact tracers from land with a 15 or 30 day lifetime, as shown in panels (c) and (e) of Fig. 10. There are also similarities in the spatial distributions of HDD in panels (b), (d), and (f) of Fig. 4 and those for the surface contact tracers from ocean with a 15 or 30 day lifetime, as shown in panels (d) and (f) of Fig. 10. The relative strength of linear relationships between seasonal cycle parameters from OCO-2 observations and surface contact tracers are quantified with correlation coefficients in Fig. 11. The higher correlation coefficients obtained when comparing SCA to land and ocean tracers with 15 day and 30 day lifetimes suggest that accumulation of CO<sub>2</sub> flux due to atmospheric transport on roughly monthly timescales plays an important role in defining  $X_{CO_2}$  SCA.

Correlations between HDD and land tracers are weak, which is unexpected given the close correlation between HDD from terrestrial NEE and HDD from  $X_{CO_2}$  in Fig. 9 panel (b). Relationships between HDD and land and ocean tracers seem to



follow a curve rather than a line, or may be representative of two different linear relationships for different groups of zones (see supplement Fig. S31). The correlations with ocean tracers were always inverted relative to those with land tracers, such that reduced contribution from ocean tracers and increased contributions from land tracers consistently correspond with larger SCA and often correspond with earlier HDD (see supplement Fig. S31). The relatively strong correlations between land tracers and SCA is consistent with the finding in Sect. 4.1 that terrestrial biospheric exchange is the dominant driver of seasonality in  $X_{CO_2}$ .

### 4.3 The role of $CO_2$ fluxes in $X_{CO_2}$ SCA

The role of fluxes within each  $5^\circ$  latitude by  $20^\circ$  longitude zone in determining the  $X_{CO_2}$  SCA are assessed here using flux estimates from the same model frameworks that are used for previous comparisons of  $X_{CO_2}$  SCA in this analysis. The GEOS-Chem  $CO_2$  simulation uses a combination of flux inventories (Hoesly et al., 2018; Randerson et al., 2018; van der Werf et al., 2017) and CarbonTracker2019 (Jacobson et al., 2020) biospheric fluxes from land and ocean, while the CAMS v19r1 model framework includes a flux inversion that is internally consistent with model estimates of  $X_{CO_2}$  (Chevallier, 2020b). To obtain the estimated  $CO_2$  flux for GEOS-Chem, the fossil fuel, biomass burning, and biospheric fluxes are summed together. First,  $CO_2$  fluxes from each model are averaged spatially within zones for each 3-hourly time-step. A total average annual flux is calculated for each zone by summing all 3-hourly  $CO_2$  fluxes in each year and taking an average over the six years in 2014-2019. To calculate flux SCA, the daily sums of 3-hourly, spatially-averaged fluxes within each zone are used to derive a 15-day rolling mean, which is then averaged by day of year to yield an average annual cycle, and the difference between the maximum and minimum of the average annual cycle is taken to be the flux SCA. The annual cycles of fluxes are plotted in Figures S32 through S49.

Figure 12 has maps of average annual fluxes and flux SCA for GEOS-Chem and CAMS, which show that flux SCA in panels (a) and (b) are distributed following more of a meridional gradient and less of a longitudinal gradient than  $X_{CO_2}$  SCA in panels (a), (c), and (e) of Fig. 4. The weak correlations between flux SCA and  $X_{CO_2}$  SCA, shown in panels (a), (b), and (c) of Fig. 13 and quantified in Fig. 14, combined with the relatively strong correlations between  $X_{CO_2}$  and surface contact tracers with 15 and 30 day lifetimes, suggest that accumulation of  $CO_2$  flux due to atmospheric transport on roughly monthly timescales is more influential in determining  $X_{CO_2}$  SCA than fluxes within a  $5^\circ$  latitude by  $20^\circ$  longitude zone. However, there are slightly stronger correlations between average annual flux and  $X_{CO_2}$  SCA, shown in panels (d), (e), and (f) of Fig. 13 and quantified in Fig. 14, which suggest some possible link between  $X_{CO_2}$  SCA and the relative source or sink strength of a given zone. Panels (c) and (d) of Fig. 12 show that both models predict large negative average annual fluxes for Asian Boreal zones, designating the Asian Boreal region as a major sink for  $CO_2$ , and suggesting that anomalously large  $X_{CO_2}$  SCA in the Asian Boreal region may be partially influenced by enhancements in  $CO_2$  uptake within that region. In another instance, the European Temperate zone 3 and Bremen TCCON site both have exceptionally large positive average annual  $CO_2$  flux due to a significant contribution from fossil fuel emissions (as shown in Sect. S4), but they did not yield anomalously large flux SCA because the fossil fuel emissions do not exhibit any significant seasonal variability. The European Temperate zone 3 and Bremen also yielded smaller  $X_{CO_2}$  SCA and later HDD than most of the other zones and ground sites for both observed and



model-derived seasonal cycles. In this case, the large fossil fuel emissions may be indirectly influencing the  $X_{CO_2}$  SCA despite the fact that these emissions are not directly contributing to the seasonal variability in atmospheric  $CO_2$  in this zone or at this site.

## 5 Conclusions

5 Satellite-based instruments, such as OCO-2, open the possibility to study  $CO_2$  exchange and transport throughout the vast and largely un-instrumented northern high latitudes. Improvements in retrieval and quality control methods for satellite-based observations of atmospheric  $CO_2$  have allowed for a data-driven investigation of  $X_{CO_2}$  seasonality over regions, like Siberia, that have previously been largely inaccessible and unobserved. Our results show that the Asian Boreal Forest region is distinct from other northern high latitude regions with larger seasonal cycle amplitude (SCA) and earlier half drawdown day (HDD)  
10 (see Sect. 2.6), and gradients of increasing SCA and earlier HDD span from west to east across the Eurasian continent. Longitudinal gradients in SCA and HDD across the North American continent are more subtle than longitudinal gradients across the Eurasian continent. Discrepancies between observed (OCO-2) and model-derived (CAM5 and GEOS-Chem) SCA and HDD in the eastern zones of North America result in opposing longitudinal gradients in SCA and HDD across the North American continent, such that OCO-2 observations yield increasing SCA from east to west, while model estimates yield increasing SCA  
15 from west to east. In order to assess the relative influences of the accumulation of  $CO_2$  exchanges during atmospheric transport or the magnitudes of fluxes within  $5^\circ$  latitude by  $20^\circ$  longitude zones, we compare GEOS-Chem  $CO_2$  source apportionment and GEOS-Chem surface contact tracers with observed spatial distributions of SCA and HDD from OCO-2. GEOS-Chem simulated source contributions of NEE to  $X_{CO_2}$  yield nearly the same seasonal cycles as  $X_{CO_2}$ , while other source contributions exhibit little to no seasonal variability, suggesting that the seasonality in  $X_{CO_2}$  over northern high latitudes can be attributed  
20 almost entirely to terrestrial biospheric exchange. The dominance of terrestrial biospheric exchange in the GEOS-Chem model is likely an intentional quality built into the model, but the strong correlations between observed and GEOS-Chem-derived seasonal cycle parameters lend some credence to the assumptions made in the GEOS-Chem  $CO_2$  simulation. GEOS-Chem surface contact tracers revealed that the largest  $X_{CO_2}$  SCA occur in areas with the greatest influence from land tracers with 15 or 30 lifetimes. The correlations of  $X_{CO_2}$  SCA with land contact tracers are stronger than the correlations of  $X_{CO_2}$  SCA  
25 with SCA of  $CO_2$  fluxes within a given  $5^\circ$  latitude by  $20^\circ$  longitude zone. This indicates that accumulation of terrestrial  $CO_2$  flux during atmospheric transport on roughly monthly timescales is a major driver of regional variations in  $X_{CO_2}$  SCA, which is at least as important in shaping observed  $X_{CO_2}$  seasonality as the terrestrial flux magnitudes within zones. However, there is some correlation between the total average annual fluxes used in the GEOS-Chem  $CO_2$  simulation and  $X_{CO_2}$  SCA, and the Asian Boreal region was still determined to have by far the largest negative fluxes of any of the regions in addition to having  
30 the largest  $X_{CO_2}$  SCA and earliest HDD. Our overall conclusions are that a combination of the magnitudes of fluxes within zones and the accumulation of  $CO_2$  flux during atmospheric transport defines the observed spatial distributions of  $X_{CO_2}$  seasonal cycle parameters, a robust understanding of atmospheric transport patterns on roughly monthly timescales is essential for accurate interpretation of  $X_{CO_2}$  seasonality for northern high latitudes, and seasonality in  $X_{CO_2}$  in northern high latitude



regions is almost completely dictated by seasonality in the exchange of CO<sub>2</sub> with the terrestrial biosphere. In future work, it would of value to expand this analysis to assess both long-term temporal trends in  $X_{CO_2}$  seasonality, as well as interannual anomalies that may result from global weather patterns such as the polar vortex or el niño.

5

*Code and data availability.* OCO-2 data and quality control parameters used here are taken from OCO-2 Lite files (version 9, "B9"), and quality filtering and bias corrections are applied following Jacobs et al. (2020b), as described in Sect. 2.1. OCO-2 Lite files are produced by the NASA OCO-2 project at the Jet Propulsion Laboratory, California Institute of Technology, and obtained from the NASA Goddard Earth Science Data and Information Services Center (GES-DISC; <https://daac.gsfc.nasa.gov/>). TCCON data are available from the TCCON data archive, hosted by CaltechDATA: <https://tccodata.org/>. EM27/SUN GGG2014 retrievals from Fairbanks, Alaska are available on the Oak Ridge National Laboratory Distributed Active Archive Center (ORNL DAAC): <https://doi.org/10.3334/ORNLDAAC/1831> [these data may still be in the process of being published to the ORNL DAAC, but are expected to be available by the time of manuscript acceptance]. Methods used to bias correct EM27/SUN data to TCCON are described in the supplemental materials for Jacobs et al. (2020b). All ground-based datasets are also cited individually in Sect. 2.2. CAMS optimized flux-inversion model output is available on the Copernicus website: <https://ads.atmosphere.copernicus.eu/cdsapp#!/dataset/cams-global-greenhouse-gas-inversion>. GEOS-Chem source code is publicly available (<https://doi.org/10.5281/zenodo.3701669>). Model output analyzed in this work are archived at Zenodo [data in netCDF format will be uploaded after manuscript acceptance].

20

*Author contributions.* Nicole Jacobs composed this manuscript and conducted the analysis under the supervision of William R. Simpson. Kelly A. Graham and Christopher Holmes ran GEOS-Chem simulations and provided essential guidance in interpreting results. Frank Hase,





Thomas Blumenstock, Qiansi Tu, Matthias Frey, Manvendra K. Dubey, and Harrison A. Parker all contributed to data collection with the EM27/SUNs in Fairbanks, including instrument evaluations, maintenance, and establishing long-term operations in Fairbanks. Debra Wunch contributed data from the East Trout Lake TCCON site, as well as a thorough evaluation of the manuscript. Rigel Kivi and Pauli Heikkinen contributed data from the Sodankylä TCCON site. Justus Notholt, Christof Petri, and Thorsten Warneke contributed data from the Białystok and Bremen TCCON sites. All coauthors have provided essential feedback and insights on the content of the manuscript and supplemental materials.

*Competing interests.* The authors declare that they have no conflict of interest.

*Acknowledgements.* The Simpson Lab at UAF acknowledges the Alaska Space Grant Graduate Fellowship and OCO Science Team Grant (NNH17ZDA001N-OCO2) for support. K. A. Graham and C. Holmes acknowledge support from the NSF Office of Polar Programs (grant 1602883) and the NASA Earth and Space Science Fellowship (grant 80NSSC17K0361). KIT acknowledges support by ESA via the projects COCCON-PROCEEDS, COCCON-PROCEEDS II, and FRM4GHG. M. K. Dubey thanks NASA CMS, LANL LDRD and UCOP support for the LANL EM27/SUN deployments. D. Wunch acknowledges CFI, ORF, and NSERC support for the ETL TCCON station.



## References

- Barlow, J. M., Palmer, P. I., Bruhwiler, L. M., and Tans, P.: Analysis of CO<sub>2</sub> mole fraction data: first evidence of large-scale changes in CO<sub>2</sub> uptake at high northern latitudes, *Atmos. Chem. Phys.*, 15, 13 739–13 758, <https://doi.org/10.5194/acp-15-13739-2015>, [www.atmos-chem-phys.net/15/13739/2015/](http://www.atmos-chem-phys.net/15/13739/2015/), 2015.
- 5 Barnes, E. A., Parazoo, N., Orbe, C., and Denning, A. S.: Isentropic transport and the seasonal cycle amplitude of CO<sub>2</sub>, *J. Geophys. Res.-Atmos.*, 121, 8106–8124, <https://doi.org/10.1002/2016JD025109>, 2016.
- Bastos, A., Ciaï, P., Chevallier, F., Rödenbeck, C., Ballantyne, A. P., Maignan, F., Yin, Y., Fernández-Martínez, M., Friedlingstein, P., Peñuelas, J., Piao, S. L., Sitch, S., Smith, W. K., Wang, X., Zhu, Z., Haverd, V., Kato, E., Jain, A. K., Lienert, S., Lombardozzi, D., Nabel, J. E. M. S., Peylin, P., Poulter, B., and Zhu, D.: Contrasting effects of CO<sub>2</sub> fertilization, land-use change and warming on seasonal  
10 amplitude of Northern Hemisphere CO<sub>2</sub> exchange, *Atmos. Chem. Phys.*, 19, 12 361–12 375, <https://doi.org/10.5194/acp-19-12361-2019>, 2019.
- Basu, S., Guerlet, S., Butz, A., Houweling, S., Hasekamp, O., Aben, I., Krummel, P., Steele, P., Langenfelds, R., Torn, M., Biraud, S., Stephens, B., Andrews, A., and Worthy, D.: Global CO<sub>2</sub> fluxes estimated from GOSAT retrievals of total column CO<sub>2</sub>, *Atmos. Chem. Phys.*, 13, 8695–8717, <https://doi.org/10.5194/acp-13-8695-2013>, 2013.
- 15 Bovensmann, H., Burrows, J. P., Buchwitz, M., Frerick, J., Noël, S., Rozanov, V. V., Chance, K. V., and Goede, A. P. H.: SCIAMACHY: Mission Objectives and Measurement Modes, *J. Atmos. Sci.*, 56, 127–150, [https://doi.org/10.1175/1520-0469\(1999\)056<0127:smoamm>2.0.co;2](https://doi.org/10.1175/1520-0469(1999)056<0127:smoamm>2.0.co;2), 1999.
- Bradshaw, C. J. A. and Warkentin, I. G.: Global estimates of boreal forest carbon stocks and flux, *Global Planet Change*, 128, 24–30, <https://doi.org/10.1016/j.gloplacha.2015.02.004>, 2015.
- 20 Bukosa, B.: Modelling of Greenhouse Gases in Australia and the Globe on Multiple Scales, <https://ro.uow.edu.au/theses/1731>, 2019.
- Burrows, J. P., Holzie, E., Goede, A. P. H., Visser, H., and Fricke, W.: SCIAMACHY-Scanning Imaging Absorption Spectrometer for Atmospheric Cartography, *Acta Astronaut.*, 35, 445–451, [https://doi.org/10.1016/0094-5765\(94\)00278-T](https://doi.org/10.1016/0094-5765(94)00278-T), 1995.
- Byrne, B., Wunch, D., Jones, D. B. A., Strong, K., Deng, F., Baker, I., Köhler, P., Frankenberg, C., Joiner, J., Arora, K., Badawy, B., Harper, A. B., Warneke, T., Petri, C., Kivi, R., and Roehl, C. M.: Evaluating GPP and Respiration Estimates Over Northern Midlatitude Ecosystems Using Solar-Induced Fluorescence and Atmospheric CO<sub>2</sub> Measurements, *J. Geophys. Res.-Biogeophys.*, 123, 2976–2997,  
25 <https://doi.org/10.1029/2018JG004472>, 2018.
- Chevallier, F.: Validation report for the CO<sub>2</sub> fluxes estimated by atmospheric inversion, v19r1 Version 1.0, [https://atmosphere.copernicus.eu/sites/default/files/2020-08/CAMS73\\_2018SC2\\_D73.1.4.1-2019-v1\\_202008\\_v3-1.pdf](https://atmosphere.copernicus.eu/sites/default/files/2020-08/CAMS73_2018SC2_D73.1.4.1-2019-v1_202008_v3-1.pdf), 2020a.
- Chevallier, F.: Description of the CO<sub>2</sub> inversion production chain 2020 Version 1.0, [https://atmosphere.copernicus.eu/sites/default/files/2020-06/CAMS73\\_2018SC2\\_%20D5.2.1-2020\\_202004\\_%20CO2%20inversion%20production%20chain\\_v1.pdf](https://atmosphere.copernicus.eu/sites/default/files/2020-06/CAMS73_2018SC2_%20D5.2.1-2020_202004_%20CO2%20inversion%20production%20chain_v1.pdf), 2020b.
- 30 Crisp, D., Pollock, H. R., Rosenberg, R., Chapsky, L., Lee, R. A. M., Oyafuso, F. A., Frankenberg, C., O'Dell, C. W., Bruegge, C. J., Doran, G. B., Eldering, A., Fisher, B. M., Fu, D., Gunson, M. R., Mandrake, L., Osterman, G. B., Schwandner, F. M., Sun, K., Taylor, T. E., Wennberg, P. O., and Wunch, D.: The on-orbit performance of the Orbiting Carbon Observatory-2 (OCO-2) instrument and its radiometrically calibrated products, *Atmos. Meas. Tech.*, 10, 59–81, <https://doi.org/10.5194/amt-10-59-2017>, 2017.
- 35 Deutscher, N. M., Notholt, J., Messerschmidt, J., Weinzierl, C., Warneke, T., Petri, C., and Grupe, P.: TCCON data from Bialystok (PL), Release GGG2014.R2 (Version R2) TCCON data archive, hosted by CaltechDATA, California Institute of Technology, Pasadena, CA, U.S.A., <https://doi.org/10.14291/tcon.ggg2014.bialystok01.R2>, <https://doi.org/10.14291/TCCON.GGG2014.BIALYSTOK01.R2>, 2019.



- Euskirchen, E. S., McGuire, A. D., and Chapin III, F. S.: Energy feedbacks of northern high-latitude ecosystems to the climate system due to reduced snow cover during 20th century warming, *Glob. Change Biol.*, 13, 2425–2438, <https://doi.org/10.1111/j.1365-2486.2007.01450.x>, 2007.
- Euskirchen, E. S., Edgar, C. W., Bret-Harte, M. S., Kade, A., Zimov, N., and Zimov, S.: Interannual and Seasonal Patterns of Carbon Dioxide, Water, and Energy Fluxes From Ecotonal and Thermokarst-Impacted Ecosystems on Carbon-Rich Permafrost Soils in Northeastern Siberia, *J. Geophys. Res.-Biogeo.*, 122, 2651–2668, <https://doi.org/10.1002/2017JG004070>, 2017.
- Forkel, M., Carvalhais, N., Rödenbeck, C., Keeling, R., Heimann, M., Thonicke, K., Zaehle, S., and Reichstein, M.: Enhanced seasonal CO<sub>2</sub> exchange caused by amplified plant productivity in northern ecosystems, *Science*, 351, 696–699, <https://doi.org/10.1126/science.aac4971>, 2016.
- 5 Frey, M., Sha, M. K., Hase, F., Kiel, M., Blumenstock, T., Harig, R., Surawicz, G., Deutscher, N. M., Shiomi, K., Franklin, J. E., Bösch, H., Chen, J., Grutter, M., Ohshima, H., Sun, Y., Butz, A., Mengistu Tsidu, G., Ene, D., Wunch, D., Cao, Z., Garcia, O., Ramonet, M., Vogel, F., and Orphal, J.: Building the Collaborative Carbon Column Observing Network (COCCON): long-term stability and ensemble performance of the EM27/SUN Fourier transform spectrometer, *Atmos. Meas. Tech.*, 12, 1513–1530, <https://doi.org/10.5194/amt-12-1513-2019>, 2019.
- 15 Gauthier, S., Bernier, P., Kuuluvainen, T., Shvidenko, A. Z., and Schepaschenko, D. G.: Boreal forest health and global change, *Science*, 349, 819–822, <https://doi.org/10.1126/science.aaa9092>, 2015.
- Gelaro, R., McCarty, W., Suárez, M. J., Todling, R., Molod, A., Takacs, L., Randles, C. A., Darmenov, A., Bosilovich, M. G., Reichle, R., Krzyztof, W., Coy, L., Cullather, R., Draper, C., Akella, S., Buchard, V., Conaty, A., da Silva, A. M., Gu, W., Kim, G.-K., Koster, R., Lucchesi, R., Merkova, D., Nielson, J. E., Partyka, G., Pawson, S., Putman, W., Rienecker, M., Schubert, S. D., Sienkiewicz, M., and Zhao, B.: The Modern-Era Retrospective Analysis for Research and Applications, Version 2 (MERRA-2), *J. Climate*, 30, 5419–5454, <https://doi.org/10.1175/JCLI-D-16-0758.1>, 2017.
- 20 Gisi, M., Hase, F., Dohe, S., Blumenstock, T., Simon, A., and Keens, A.: X<sub>CO2</sub>-measurements with a tabletop FTS using solar absorption spectroscopy, *Atmos. Meas. Tech.*, 5, 2969–2980, <https://doi.org/10.5194/amt-5-2969-2012>, 2012.
- Graven, H. D., Keeling, R. F., Piper, S. C., Patra, P. K., Stephens, B. B., Wofsy, S. C., Welp, L. R., Sweeney, C., Tans, P. P., Kelley, J. J., Daube, B. C., Kort, E. A., Santoni, G. W., and Bent, J. D.: Enhanced Seasonal Exchange of CO<sub>2</sub> by Northern Ecosystems Since 1960, *Science*, 341, <https://doi.org/10.1126/science.1239207>, 2013.
- Gray, J. M., Frolking, S., Kort, E. A., Ray, D. K., Kucharik, C. J., Ramankutty, N., and Friedl, M. A.: Direct human influence on atmospheric CO<sub>2</sub> seasonality from increased cropland productivity, *Nature*, 515, 398–401, <https://doi.org/10.1038/nature13957>, 2014.
- Gurney, K., Law, R., and Rayner, P.: TransCom 3 experimental protocol, Dept. of Atmos. Sci., Colo. State Univ., [https://www.researchgate.net/profile/Kevin\\_Gurney2/publication/228955926\\_TransCom\\_3\\_Experimental\\_Protocol/links/00b7d515d0402af968000000/TransCom-3-Experimental-Protocol.pdf](https://www.researchgate.net/profile/Kevin_Gurney2/publication/228955926_TransCom_3_Experimental_Protocol/links/00b7d515d0402af968000000/TransCom-3-Experimental-Protocol.pdf), 2000.
- 30 Hamazaki, T., Kaneko, Y., Kuze, A., and Kondo, K.: Fourier transform spectrometer for Greenhouse Gases Observing Satellite (GOSAT), in: Proc. SPIE 5659, Enabling Sensor and Platform Technologies for Spaceborne Remote Sensing, <https://doi.org/10.1117/12.581198>, 2005.
- Hayes, D. J., McGuire, A. D., Kicklighter, D. W., Gurney, K. R., Burnside, T. J., and Melillo, J. M.: Is the northern high-latitude land-based CO<sub>2</sub> sink weakening?, *Global Biogeochem. Cy.*, 25, <https://doi.org/10.1029/2010GB003813>, 2011.
- Hedelius, J. and Wennberg, P.: EM27/SUN GGG interferogram processing suite Version 2014, Hosted on CaltechDATA data archive, California Institute of Technology, Pasadena, California, U.S.A., <https://doi.org/10.22002/d1.306>, 2017.



- Hedelius, J. K., Parker, H., Wunch, D., Roehl, C. M., Viatte, C., Newman, S., Toon, G. C., Podolske, J. R., Hillyard, P. W., Iraci, L. T., Dubey, M. K., and Wennberg, P. O.: Intercomparability of XCO and XCH<sub>4</sub> from the United and States and TCCON sites, *Atmos. Meas. Tech.*, 10, 1481–1493, <https://doi.org/10.5194/amt-10-1481-2017>, [www.atmos-meas-tech.net/10/1481/2017/](http://www.atmos-meas-tech.net/10/1481/2017/), 2017.
- 5 Hoesly, R. M., Smith, S. J., Feng, L., Klimont, Z., Janssens-Maenhout, G., Pitkanen, T., Seibert, J. J., Vu, L., Andres, R. J., Bolt, R. M., Bond, T. C., Dawidowski, L., Kholod, N., Kurokawa, J.-I., Li, M., Liu, L., Lu, Z., Moura, M. C. P., O'Rourke, P. R., and Zhang, Q.: Historical (1750-2014) anthropogenic emissions of reactive gases and aerosols from the Community Emissions Data System (CEDS), *Geosci. Model Dev.*, 11, 369–408, <https://doi.org/doi.org/10.5194/gmd-11-369-2018>, 2018.
- Holland, M. M. and Bitz, C. M.: Polar amplification of climate change in coupled models, *Clim. Dynam.*, 21, 221–232, <https://doi.org/10.1007/s00382-003-0332-6>, 2003.
- 10 Jacobs, N., Simpson, W. R., Hase, F., Blumenstock, T., Tu, Q., Frey, M., Dubey, M. K., and Parker, H.: <https://doi.org/10.3334/ORNLDAAAC/1831>, 2020a.
- Jacobs, N., Simpson, W. R., Wunch, D., O'Dell, C. W., Osterman, G. B., Hase, F., Blumenstock, T., Tu, Q., Frey, M., Dubey, M. K., Parker, H. A., Kivi, R., and Heikkinen, P.: Quality controls, bias, and seasonality of CO<sub>2</sub> columns in the boreal forest with Orbiting Carbon Observatory-2, Total Carbon Column Observing Network, and EM27/SUN measurements, *Atmos. Meas. Tech.*, 13, 5033–5063, <https://doi.org/10.5194/amt-13-5033-2020>, 2020b.
- 15 Jacobson, A. R., Schuldt, K. N., Miller, J. B., Oda, T., Tans, P., Andrews, A., Mund, J., Ott, L., Collatz, G. J., Aalto, T., Afshar, S., Aikin, K., Aoki, S., Apadula, F., Baier, B., Bergamaschi, P., Beyersdorf, A., Biraud, S. C., Bollenbacher, A., Bowling, D., Brailsford, G., Abshire, J. B., Chen, G., Chen, H., Chmura, L., Climadat, S., Colomb, A., Conil, S., Cox, A., Cristofanelli, P., Cuevas, E., Curcoll, R., Sloop, C. D., Davis, K., De Wekker, S., Delmotte, M., DiGangi, J. P., Dlugokencky, E., Ehleringer, J., Elkins, J. W., Emmenegger, L., Fischer, M. L., Forster, G., Frumau, A., Galkowski, M., Gatti, L. V., Gloor, E., Griffis, T., Hammer, S., Haszpra, L., Hatakka, J., Heliasz, M., Hensen, A., Hermanssen, O., Hintsa, E., Holst, J., Jaffe, D., Karion, A., Kawa, S. R., Keeling, R., Keronen, P., Kolari, P., Kominkova, K., Kort, E., Krummel, P., Kubistin, D., Labuschagne, C., Langenfelds, R., Laurent, O., Laurila, T., Lauvaux, T., Law, B., Lee, J., Lehner, I., Leuenberger, M., Levin, I., Levula, J., Lin, J., Lindauer, M., Loh, Z., Lopez, M., Myhre, C. L., Machida, T., Mammarella, I., Manca, G., Manning, A., Manning, A., Marek, M. V., Marklund, P., Martin, M. Y., Matsueda, H., McKain, K., Meijer, H., Meinhardt, F., Miles, N., 20 Miller, C. E., Mölder, M., Montzka, S., Moore, F., Morgui, J.-A., Morimoto, S., Munger, B., Necki, J., Newman, S., Nichol, S., Niwa, Y., O'Doherty, S., Ottosson-Löfvenius, M., Paplawsky, B., Peischl, J., Peltola, O., Pichon, J.-M., Piper, S., Plass-Dölmer, C., Ramonet, M., Reyes-Sanchez, E., Richardson, S., Riris, H., Ryerson, T., Saito, K., Sargent, M., Sasakawa, M., Sawa, Y., Say, D., Scheeren, B., Schmidt, M., Schmidt, A., Schumacher, M., Shepson, P., Shook, M., Stanley, K., Steinbacher, M., Stephens, B., Sweeney, C., Thoning, K., Torn, M., Turnbull, J., Tørseth, K., van den Bulk, P., van der Laan-Luijkx, I. T., van Dinter, D., Vermeulen, A., Viner, B., Vitkova, G., Walker, S., Weyrauch, D., Wofsy, S., Worthy, D., Young, D., and Zimnoch, M.: CarbonTracker Documentation CT2019 release, [https://www.esrl.noaa.gov/gmd/ccgg/carbontracker/CT2019\\_doc.php](https://www.esrl.noaa.gov/gmd/ccgg/carbontracker/CT2019_doc.php), 2020.
- 30 Keppel-Aleks, G., Wennberg, P. O., Washenfelder, R. A., Wunch, D., Schneider, T., Toon, G. C., Andres, R. J., Blavier, J.-F., Connor, B., Davis, K. J., Desai, A. R., Messerschmidt, J., Notholt, J., Roehl, C. M., Sherlock, V., Stephens, B. B., Vay, S. A., and Wofsy, S. C.: The imprint of surface fluxes and transport on variations in total column carbon dioxide, *Biogeosciences*, 9, 875–891, <https://doi.org/10.5194/bg-9-875-2012>, 2012.
- 35 Kiel, M., O'Dell, C. W., Fisher, B., Eldering, A., Nassar, R., MacDonald, C. G., and Wennberg, P. O.: How bias correction goes wrong: measurement of X<sub>CO<sub>2</sub></sub> affected by erroneous surface pressure estimates, *Atmos. Meas. Tech.*, 12, 2241–2259, <https://doi.org/10.5194/amt-12-2241-2019>, 2019.



- Kivi, R. and Heikkinen, P.: Fourier transform spectrometer measurements of column CO<sub>2</sub> at Sodankylä, Finland, *Geosci. Instrum. Method. Data Syst.*, 5, 271–279, <https://doi.org/10.5194/gi-5-271-2016>, 2016.
- Kivi, R., Heikkinen, P., and Kyrö, E.: TCCON data from Sodankylä (FI), Release GGG2014.R0 (Version GGG2014.R0). TCCON data archive, hosted by CaltechDATA, California Institute of Technology, Pasadena, CA, U.S.A.,  
5 <https://doi.org/10.14291/tcon.ggg2014.sodankyla01.R0>, <https://doi.org/10.14291/tcon.ggg2014.sodankyla01.R0>, 2014.
- Klappenbach, F., Bertleff, M., Kostinek, J., Hase, F., Blumenstock, T., Agusti-Panareda, A., Razinger, M., and Butz, A.: Accurate mobile remote sensing of XCO<sub>2</sub> and XCH<sub>4</sub> latitudinal transects from aboard a research vessel, *Atmos. Meas. Tech.*, 8, 5023–5038, <https://doi.org/10.5194/amt-8-5023-2015>, 2015.
- Lin, X., Rogers, B. M., Sweeney, C., Chevallier, F., Arshinov, M., Dlugokencky, E., Machida, T., Sasakawa, M., Tans, P., and Keppel-Aleks,  
10 G.: Siberian and temperate ecosystems shape Northern Hemisphere atmospheric CO<sub>2</sub> seasonal amplification, *PNAS*, 117, 21 079–21 087, <https://doi.org/10.1073/pnas.1914135117>, 2020.
- Lindqvist, H., O'Dell, C. W., Basu, S., Boesch, H., Chevallier, F., Deutscher, N., Feng, L., Fisher, B., Hase, F., Inoue, M., Kivi, R., Morino, I., Palmer, P. I., Parker, R., Schneider, M., Sussmann, R., and Yoshida, Y.: Does GOSAT capture the true seasonal cycle of carbon dioxide?, *Atmos. Chem. Phys.*, 15, 13 023–13 040, <https://doi.org/10.5194/acp-15-13023-2015>, [www.atmos-chem-phys.net/15/13023/2015/](http://www.atmos-chem-phys.net/15/13023/2015/), 2015.
- 15 Liu, J., Wennberg, P. O., Parazoo, N. C., Yin, Y., and Frankenberg, C.: Observational Constraints on the Response of High-Latitude Northern Forests to Warming, *AGU Advances*, 2, <https://doi.org/10.1029/2020AV000228>, 2020.
- Manabe, S. and Wetherald, R. T.: The Effects of Doubling the CO<sub>2</sub> Concentration on the climate of a General Circulation Model, *J. Atmos. Sci.*, 32, 1975.
- Nassar, R., Jones, D. B. A., Suntharalingam, P., Chen, J. M., Andres, R. J., Wecht, K. J., Yantosca, R. M., Kulawik, S. S., Bowman,  
20 K. W., Worden, J. R., Machida, T., and Matsueda, H.: Modeling global atmospheric CO<sub>2</sub> with improved emission inventories and CO<sub>2</sub> production from the oxidation of other carbon species, *Geosci. Model Dev.*, 3, 689–716, <https://doi.org/10.5194/gmd-3-689-2010>, [www.geosci-model-dev.net/3/689/2010/](http://www.geosci-model-dev.net/3/689/2010/), 2010.
- Notholt, J., Petri, C., Warneke, T., Deutscher, N. M., Palm, M., Buschmann, M., Weinzierl, C., Macatangay, R. C., and Grupe, P.: TCCON data from Bremen (DE), Release GGG2014.R1 (Version R1) TCCON data archive, hosted by CaltechDATA, California Institute of Technology,  
25 Pasadena, CA, U.S.A., <https://doi.org/10.14291/tcon.ggg2014.bremen01.R1>, <https://doi.org/10.14291/TCCON.GGG2014.BREMEN01.R1>, 2019.
- OCO-2 Science Team/Michael Gunson, Annmarie Eldering: OCO-2 Level 2 bias-corrected XCO<sub>2</sub> and other select fields from the full-physics retrieval aggregated as daily files, Retrospective processing V9r, Greenbelt, MD, USA, Goddard Earth Sciences Data and Information Services Center (GES DISC), <https://doi.org/10.5067/W8QGIYNKS3JC>, [https://disc.gsfc.nasa.gov/datasets/OCO2\\_L2\\_Lite\\_FP\\_9r/summary](https://disc.gsfc.nasa.gov/datasets/OCO2_L2_Lite_FP_9r/summary), Accessed: [2 December 2019], 2018.
- 30 Oda, T. and Maksyutov, S.: A very high-resolution (1 km x 1 km) global fossil fuel CO<sub>2</sub> emission inventory derived using a point source database and satellite observations of nighttime lights, *Atmos. Chem. Phys.*, 11, 543–556, <https://doi.org/10.5194/acp-11-543-2011>, 2011.
- O'Dell, C. W., Eldering, A., Wennberg, P. O., Crisp, D., Gunson, M. R., Fisher, B., Frankenberg, C., Kiel, M., Lindqvist, H., Mandrake, L., Merrelli, A., Natraj, V., Nelson, R. R., Osterman, G. B., Payne, V. H., Taylor, T. E., Wunch, D., Drouin, B. J., Oyafuso, F., Chang, A., McDuffie, J., Smyth, M., Baker, D. F., Basu, S., Chevallier, F., Crowell, S. M. R., Feng, L., Palmer, P. I., Dubey, M., García, O. E., Griffith, D. W. T., Hase, F., Iraci, L. T., Kivi, R., Morino, I., Notholt, J., Ohyama, H., Petri, C., Roehl, C. M., Sha, M. K., Strong, K., Sussmann, R., Te, Y., Uchino, O., and Velazco, V.: Improved retrievals of carbon dioxide from Orbiting Carbon Observatory-2 with the version 8 ACOS algorithm, *Atmos. Meas. Tech.*, 11, 6539–6576, <https://doi.org/10.5194/amt-11-6539-2018>, 2018.



- Osterman, G. B., Eldering, A., Avis, C., Chafin, B., O'Dell, C., Frankenberg, C., Fisher, B., Mandrake, L., Wunch, D., Granat, R., and Crisp, D.: Data Product User's Guide, Operational L1 and L2 Data Versions 8 and Lite File Version 9, [https://docserver.gesdisc.eosdis.nasa.gov/public/project/OCO/OCO2\\_DUG.V9.pdf](https://docserver.gesdisc.eosdis.nasa.gov/public/project/OCO/OCO2_DUG.V9.pdf), Accessed:[8 October 2019], 2018.
- Pan, Y., Birdsey, R. A., Fang, J., Houghton, R., Kauppi, P. E., Kurz, W. A., Phillips, O. L., Shvidenko, A., Lewis, S. L., Canadell, J. G., Ciais, P., Jackson, R. B., Pacala, S. W., McGuire, A. D., Piao, S., Rautiainen, A., Sitch, S., and Hayes, D.: A Large and Persistent Carbon Sink in the World's Forests, *Science*, 333, 988–993, <https://doi.org/10.1126/science.1201609>, 2011.
- 5 P., Jackson, R. B., Pacala, S. W., McGuire, A. D., Piao, S., Rautiainen, A., Sitch, S., and Hayes, D.: A Large and Persistent Carbon Sink in the World's Forests, *Science*, 333, 988–993, <https://doi.org/10.1126/science.1201609>, 2011.
- Park, K., Kang, S. M., Kim, D., Stuecker, M. F., and Jin, F.-F.: Contrasting Local and Remote Impacts of Surface Heating on Polar Warming and Amplification, *J. Climate*, 31, 3155–3166, <https://doi.org/10.1175/JCLI-D-17-0600.1>, 2018.
- Piao, S., Liu, Z., Wang, Y., Ciais, P., Yao, Y., Peng, S., Chevallier, F., Friedlingstein, P., Janssens, I. A., Peñuelas, J., Sitch, S., and Wang, T.: On the causes of trends in the seasonal amplitude of atmospheric CO<sub>2</sub>, *Glob. Change Biol.*, 24, 608–616, <https://doi.org/10.1111/gcb.13909>, 2017.
- 10 P., Jackson, R. B., Pacala, S. W., McGuire, A. D., Piao, S., Rautiainen, A., Sitch, S., and Hayes, D.: A Large and Persistent Carbon Sink in the World's Forests, *Science*, 333, 988–993, <https://doi.org/10.1126/science.1201609>, 2011.
- Pithan, F. and Mauritsen, T.: Arctic amplification dominated by temperature feedbacks in contemporary climate models, *Nat. Geosci.*, 7, 181–184, <https://doi.org/10.1038/NGEO2071>, 2014.
- Randerson, J., van der Werf, G. R., Giglio, L., Collatz, G. J., and Kasibhatla, P. S.: Global Fire Emissions Database, Version 4.1 (GFEDv4). ORNL DAAC, Oak Ridge, Tennessee, USA, <https://doi.org/10.3334/ORNLDAAC/1293>, 2018.
- 15 ORNL DAAC, Oak Ridge, Tennessee, USA, <https://doi.org/10.3334/ORNLDAAC/1293>, 2018.
- Reuter, M., Bovensmann, H., Buchwitz, M., Burrows, J. P., Connor, B. J., Deutscher, N. M., Griffith, D. W. T., Heymann, J., Keppel-Aleks, G., Messerschmidt, J., Notholt, J., Petri, C., Robinson, J., Schneising, O., Sherlock, V., Velasco, V., Warneke, T., Wennberg, P. O., and Wunch, D.: Retrieval of atmospheric CO<sub>2</sub> with enhanced accuracy and precision from SCIAMACHY: Validation with FTS measurements and comparison with model results, *J. Geophys. Res.*, 116, <https://doi.org/10.1029/2010JD015047>, 2011.
- 20 Schneising, O., Buchwitz, M., Reuter, M., Heymann, J., Bovensmann, H., and Burrows, J. P.: Long-term analysis of carbon dioxide and methane column-averaged mole fractions retrieved from SCIAMACHY, *Atmos. Chem. Phys.*, 11, 2863–2880, <https://doi.org/10.5194/acp-11-2863-2011>, 2011.
- Schuh, A. E., Jacobson, A. R., Basu, S., Weir, B., Baker, D., Bowman, K., Chevallier, F., Crowell, S., Davis, K. J., Deng, F., Denning, S., Feng, L., Jones, D., Liu, J., and Palmer, P. I.: Quantifying the Impact of Atmospheric Transport Uncertainty on CO<sub>2</sub> Surface Flux Estimates, *Global Biogeochem. Cy.*, 33, 484–500, <https://doi.org/10.1029/2018GB006086>, 2019.
- 25 Estimates, *Global Biogeochem. Cy.*, 33, 484–500, <https://doi.org/10.1029/2018GB006086>, 2019.
- Sha, M. K., De Mazière, M., Notholt, J., Blumenstock, T., Chen, H., Dehn, A., Griffith, D. W. T., Hase, F., Heikkinen, P., Hermans, C., Hoffmann, A., Huebner, M., Jones, N., Kivi, R., Langerock, B., Petri, C., Scolas, F., Tu, Q., and Weidmann, D.: Intercomparison of low- and high-resolution infrared spectrometers for ground-based solar remote sensing measurements of total column concentrations of CO<sub>2</sub>, CH<sub>4</sub> and CO, *Atmos. Meas. Tech.*, 13, 4791–4839, <https://doi.org/10.5194/amt-13-4791-2020>, 2020.
- 30 Smith, D. M., Screen, J. A., Deser, C., Cohen, J., Fyfe, J. C., García-Serrano, J., Jung, T., Kattsov, V., Matei, D., Msadek, R., Peings, Y., Sigmund, M., Ukita, J., Yoon, J.-H., and Zhang, X.: The Polar Amplification Model Intercomparison Project (PAMIP) contribution to CMIP6: investigating the causes and consequences of polar amplification, *Geosci. Model Dev.*, 12, 1139–1164, <https://doi.org/10.5194/gmd-12-1139-2019>, 2019.
- Tans, P. P., Fung, I. Y., and Takahashi, T.: Observational Constraints on the Global Atmospheric CO<sub>2</sub> Budget, *Science*, New Series 247, 1431–1438, 1990.
- 35 Tans, P. P., Fung, I. Y., and Takahashi, T.: Observational Constraints on the Global Atmospheric CO<sub>2</sub> Budget, *Science*, New Series 247, 1431–1438, 1990.
- Thoning, K. W., Tans, P. P., and Komhyr, W. D.: Atmospheric Carbon Dioxide at Mauna Loa Observatory 2. Analysis of the NOAA GMCC Data, 1974–1985, *J. Geophys. Res.*, 94, 8549–8565, 1989.





- Tu, Q., Hase, F., Blumenstock, T., Kivi, R., Heikkinen, P., Sha, M. K., Raffalski, U., Landgraf, J., Lorente, A., Borsdorff, T., Chen, H., Dietrich, F., and Chen, J.: Intercomparison of atmospheric CO<sub>2</sub> and CH<sub>4</sub> abundances on regional scales in boreal areas using Copernicus Atmosphere Monitoring Service (CAMS) analysis, Collaborative Carbon Column Observing Network (COCCON) spectrometers, and Sentinel-5 Precursor satellite observations, *Atmos. Meas. Tech.*, 13, 4751–4771, <https://doi.org/10.5194/amt-13-4751-2020>, 2020.
- 5 van der Werf, G. R., Randerson, J. T., Giglio, L., van Leeuwen, T. T., Chen, Y., Rogers, B. M., Mu, M., van Marle, M. J. E., Morton, D. C., Collatz, G. J., Yokelson, R. J., and Kasibhatla, P. S.: Global fire emissions estimates during 1997–2016, *Earth Syst. Sci. Data*, 9, 697–720, <https://doi.org/10.5194/essd-9-697-2017>, 2017.
- Velazco, V. A., Deutscher, N. M., Morino, I., Uchino, O., Bukosa, B., Ajiro, M., Kamei, A., Jones, N. B., Paton-Walsh, C., and Griffith, D. W. T.: Satellite and Ground-based Measurements of X<sub>CO<sub>2</sub></sub> in a Remote Semi-Arid Region of Australia, *Earth Syst. Sci. Data Discuss.*,  
10 <https://doi.org/10.5194/essd-2018-161>, 2018.
- Wunch, D., Toon, G. C., Blavier, J. F. L., Washenfelder, R. A., Notholt, J., Connor, B. J., Griffith, D. W. T., Sherlock, V., and Wennberg, P. O.: The Total Carbon Column Observing Network, *Philos. T. R. Soc. A.*, 369, 2087–2112, <https://doi.org/10.1098/rsta.2010.0240>, 2011.
- Wunch, D., Wennberg, P. O., Messerschmidt, J., Parazoo, N. C., Toon, G. C., Deutscher, N. M., Keppel-Aleks, G., Roehl, C. M., Randerson, J. T., Warneke, T., and Notholt, J.: The covariation of Northern and Hemisphere summertime CO<sub>2</sub> with surface temperature in boreal regions, *Atmos. Chem. Phys.*, 13, 9447–9459, <https://doi.org/10.5194/acp-13-9447-2013>, [www.atmos-chem-phys.net/13/9447/2013/](http://www.atmos-chem-phys.net/13/9447/2013/), 2013.
- 15 Wunch, D., Wennberg, P. O., Osterman, G., Fisher, B., Naylor, B., Roehl, C. M., O’Dell, C., Mandrake, L., Viatte, C., Kiel, M., Griffith, D. W. T., Deutscher, N. M., Velazco, V. A., Notholt, J., Warneke, T., Petri, C., De Maziere, M., Sha, M. K., Sussmann, R., Rettinger, M., Pollard, D., Robinson, J., Morino, I., Uchino, O., Hase, F., Blumenstock, T., Feist, D. G., Arnold, S. G., Strong, K., Mendonca, J., Kivi, R., Heikkinen, P., Iraci, L., Podolske, J., Hillyard, P. W., Kawakami, S., Dubey, M. K., Parker, H. A., Sepulveda, E., García, O. E., Te, Y.,  
20 Jeseck, P., Gunson, M. R., Crisp, D., and Eldering, A.: Comparisons of the Orbiting Carbon Observatory-2 (OCO-2) X<sub>CO<sub>2</sub></sub> measurements with TCCON, *Atmos. Meas. Tech.*, 10, 2209–2238, <https://doi.org/10.5194/amt-10-2209-2017>, 2017.
- Wunch, D., Mendonca, J., Colebatch, O., Allen, N. T., Blavier, J.-F., Roche, S., Hedelius, J., Neufeld, G., Springett, S., Worthy, D., Kessler, R., and Strong, K.: TCCON data from East Trout Lake, SK (CA), Release GGG2014.R1 (Version R1) TCCON data archive, hosted by CaltechDATA, California Institute of Technology, Pasadena, CA, U.S.A., <https://doi.org/10.14291/tcon.ggg2014.easttroutlake01.R1>,  
25 <https://doi.org/10.14291/TCCON.GGG2014.EASTTROUTLAKE01.R1>, 2018.
- Yang, Z., Washenfelder, R. A., Keppel-Aleks, G., Krakauer, N. Y., Randerson, J. T., Tans, P. P., Sweeney, C., and Wennberg, P. O.: New constraints on Northern Hemisphere growing season net flux, *Geophys. Res. Lett.*, 34, <https://doi.org/10.1029/2007GL029742>, 2007.
- Yin, Y., Ciais, P., Chevallier, F., Li, W., Bastos, A., Piao, S., Wang, T., and Liu, H.: Changes in the Response of the Northern Hemisphere Carbon Uptake to Temperature Over the Last Three Decades, *Geophys. Res. Lett.*, 45, 4371–4380,  
30 <https://doi.org/https://doi.org/10.1029/2018GL077316>, 2018.
- Yoshida, Y., Kikuchi, N., Morino, I., Uchino, O., Oshchepkov, S., Bril, A., Saeki, T., Schutgens, N., Toon, G. C., Wunch, D., Roehl, C. M., Wennberg, P. O., Griffith, D. W. T., Deutscher, N. M., Warneke, T., Notholt, J., Robinson, J., Sherlock, V., Connor, B., Rettinger, M., Sussmann, R., Ahonen, P., Heikkinen, P., Kyrö, E., Mendonca, J., Strong, K., Hase, F., Dohe, S., and Yokota, T.: Improvement of the retrieval algorithm for GOSAT SWIR XCO<sub>2</sub> and XCH<sub>4</sub> and their validation using TCCON data, *Atmos. Meas. Tech.*, 6, 1533–1547,  
35 <https://doi.org/10.5194/amt-6-1533-2013>, 2013.
- Zeng, N., Zhao, F., Collatz, G. J., Kalnay, E., Salawitch, R. J., West, T. O., and Guanter, L.: Agricultural Green Revolution as a driver of increasing atmospheric CO<sub>2</sub> seasonal amplitude, *Nature Letters*, 515, <https://doi.org/10.1038/nature13893>, 2014.

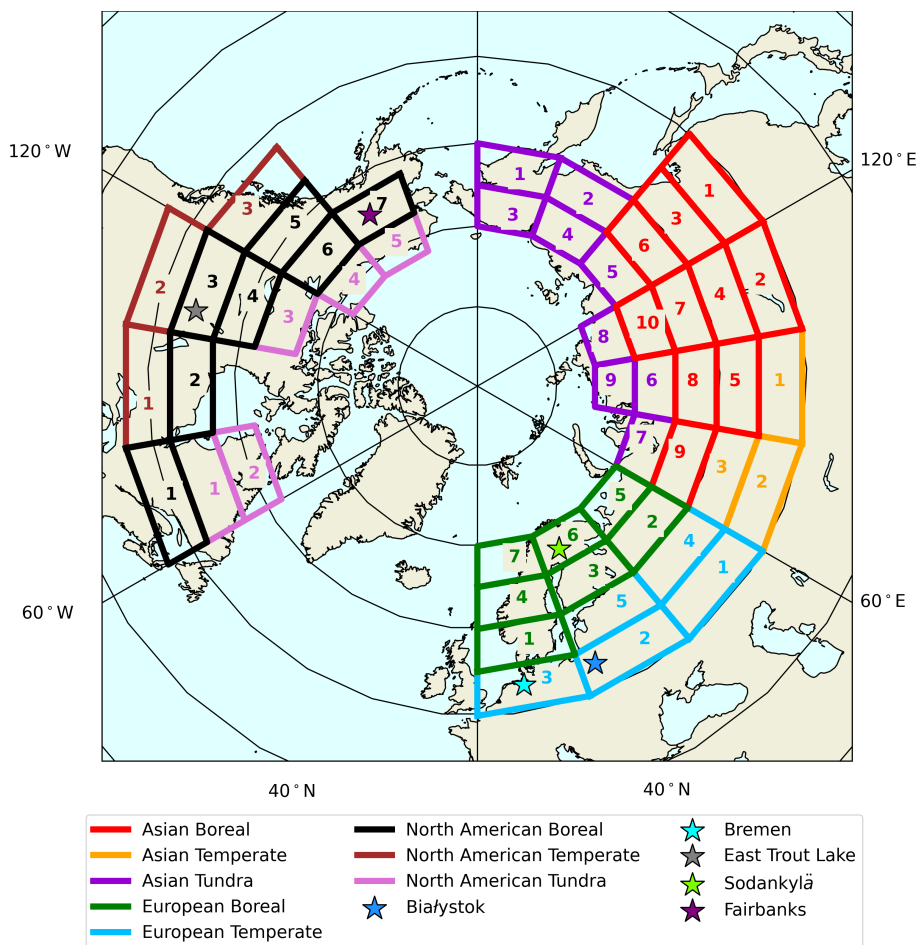


**Figure 1.** Map for of regions, zones, and locations of ground-based  $X_{CO_2}$  observations.

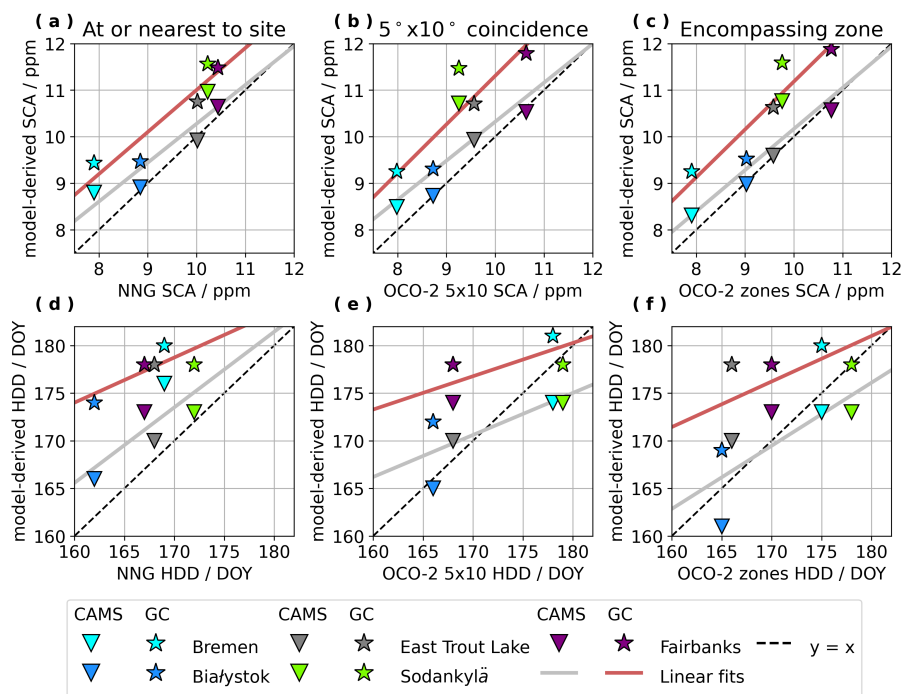


**Figure 2.** Correlations of seasonal cycle parameters from observed  $X_{CO_2}$  against seasonal cycle parameters from CAMS and GEOS-Chem model estimates. SCA and HDD are compared for three spatial types at each of the five ground sites: seasonal fits of near noon ground-based (NNG) observations from TCCON and EM27/SUN measurements are compared to fits of model-derived daily averages at the nearest model grid-point to the ground-site; fits of daily average OCO-2 retrievals that fall within the  $5^\circ$  latitude by  $10^\circ$  longitude region of coincidence, centered on the location of each ground site, are compared to fits of model-derived daily averages that fall within the coincidence region; fits of OCO-2 daily averages for the  $5^\circ$  latitude by  $20^\circ$  longitude zone containing each ground site are compared to fits of model-derived daily averages for the same zones (see map in Fig. 1 and site details in Table 1).

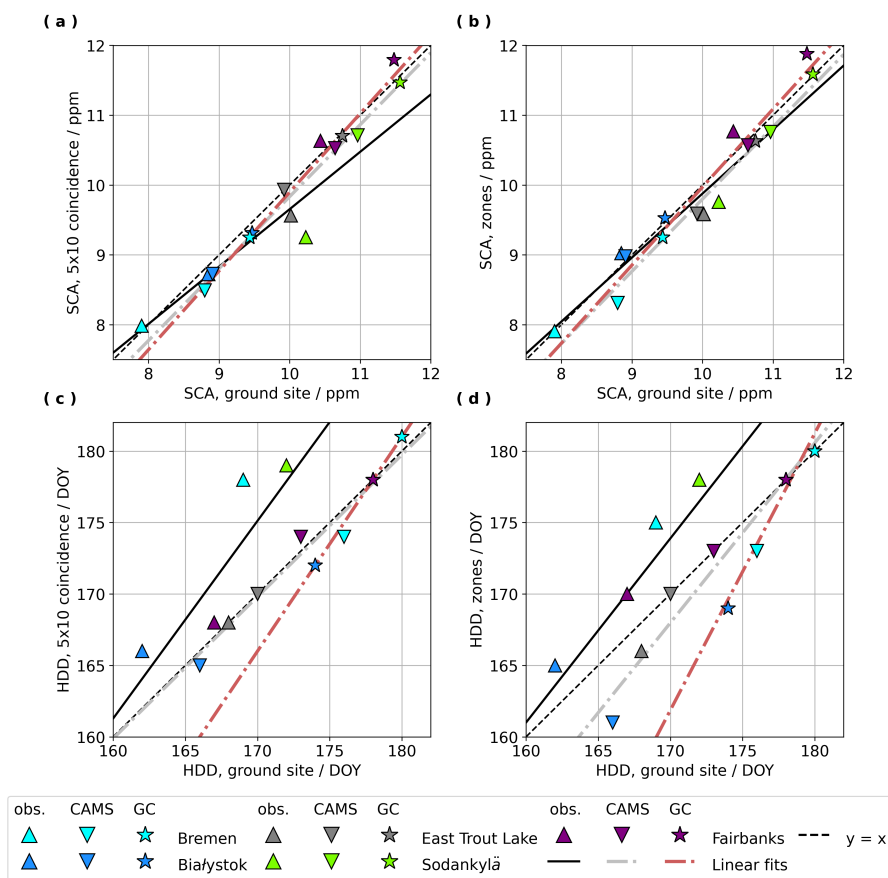


**Figure 3.** Correlations of SCA and HDD from observational and model-derived seasonal cycles at or nearest to each of five ground sites with those from seasonal cycles of spatially averaged data within the  $5^\circ$  latitude by  $10^\circ$  longitude satellite coincidence regions centered on each site and within the  $5^\circ$  latitude by  $20^\circ$  longitude zones that contains each site (not centered on the location of the site). For these correlations, we only compare across scales by pairing ground-based observations with spatially averaged OCO-2 data and pairing single-point CAMS and GEOS-Chem model estimates as near as possible to the ground sites with corresponding spatially averaged model estimates in the same model framework. Note: There are some overlapping points in the correlations of HDD in panels (c) and (d) that may visually obscure some of the results.

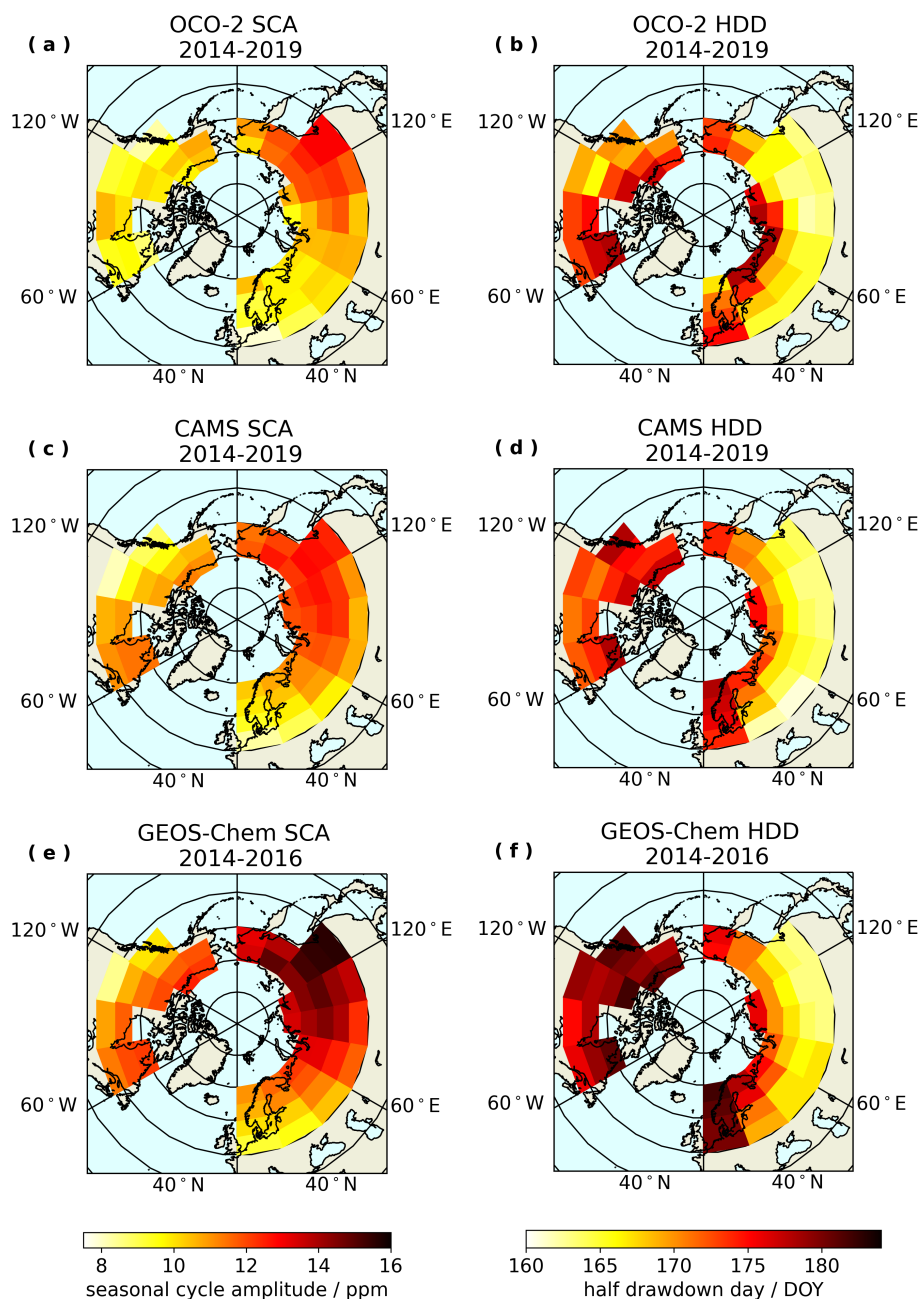


**Figure 4.** Maps of zones scaled by SCA and HDD using OCO-2, CAMS, and GEOS-Chem seasonal cycle fits.

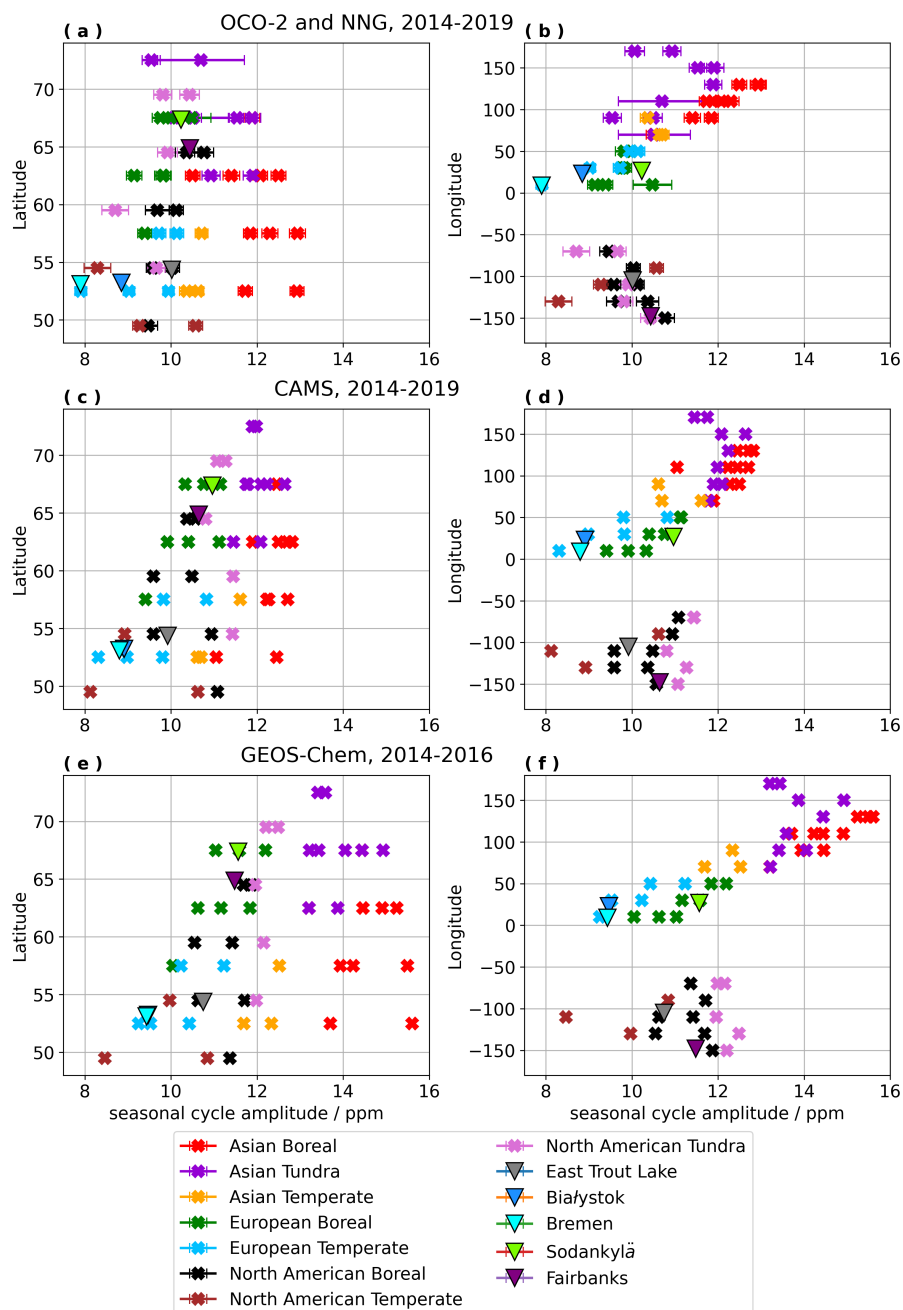


**Figure 5.** Plots of latitude and longitude correlated to SCA using observational results from OCO-2 and NNG observations ((a) and (b)), CAMS model estimates ((c) and (d)), and GEOS-Chem model estimates ((e) and (f)). The latitude and longitude for each zone is located at its center.



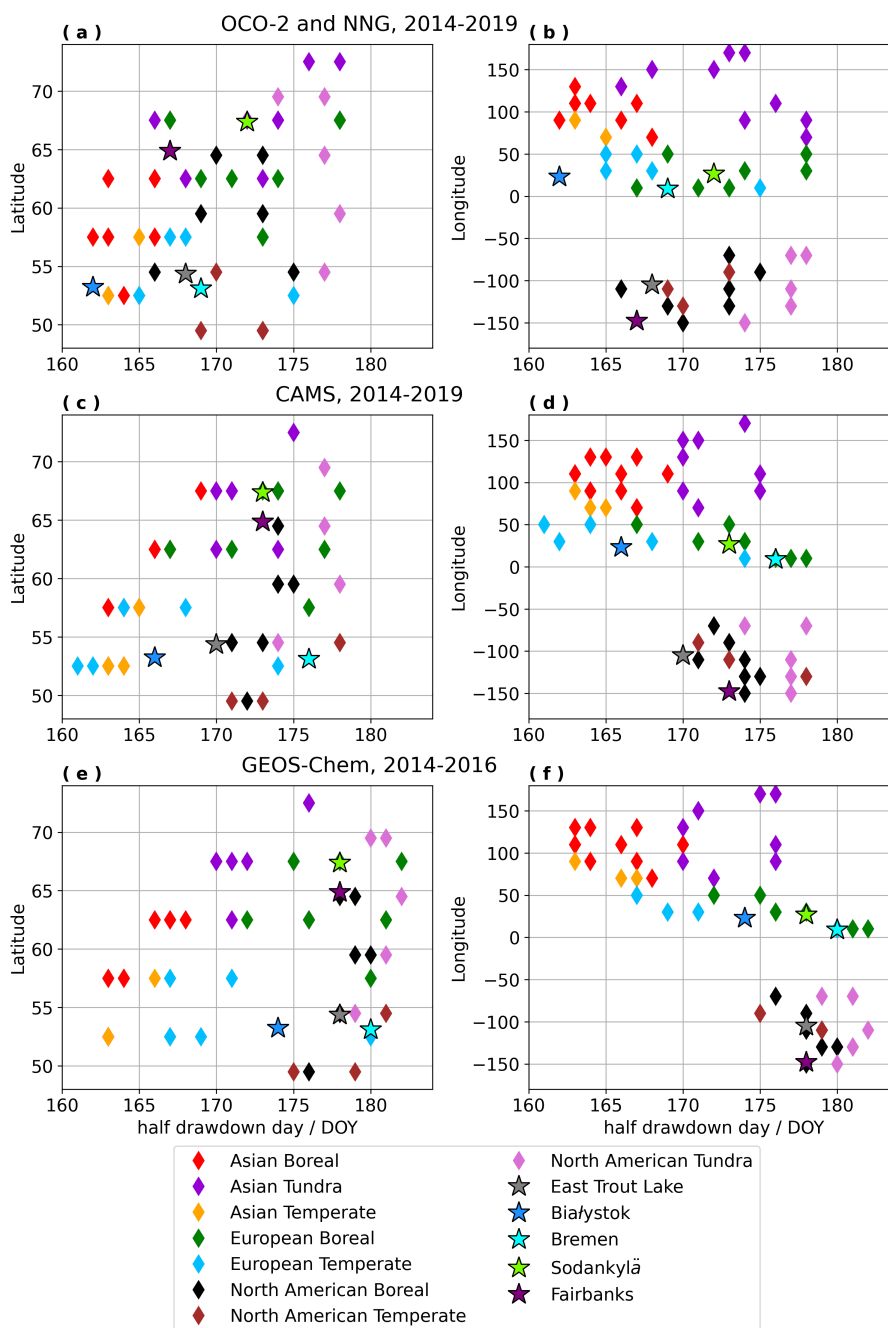


**Figure 6.** Plots of latitude and longitude correlated to HDD using observational results from OCO-2 and NNG observations ((a) and (b)), CAMS model estimates ((c) and (d)), and GEOS-Chem model estimates ((e) and (f)). The latitude and longitude for each zone is located at its center.

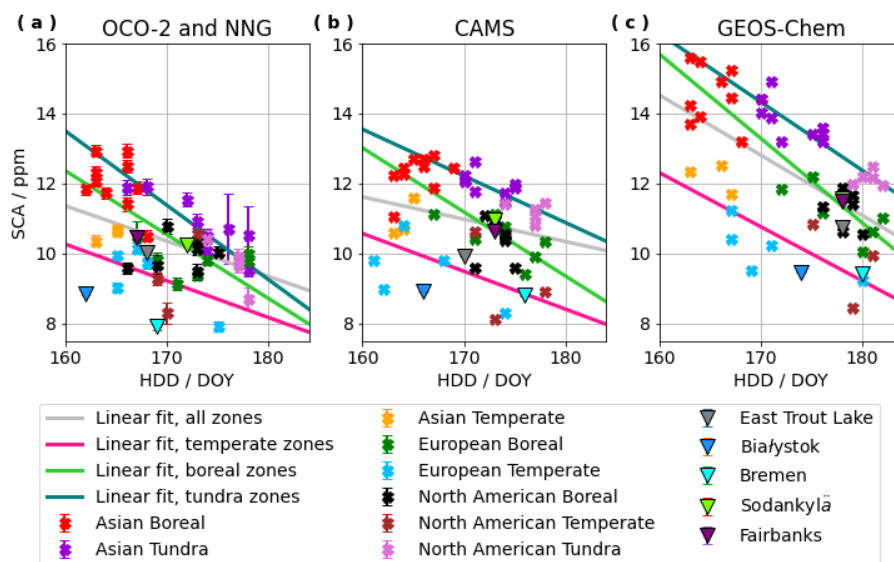


**Figure 7.** Correlations between SCA and HDD using OCO-2 and NNG seasonal cycle fits, (a), CAMS seasonal cycle fits, (b), and GEOS-Chem seasonal cycle fits (c). Linear regressions are plotted for all zones, as well as separately for Temperate, Boreal, and Tundra regions.

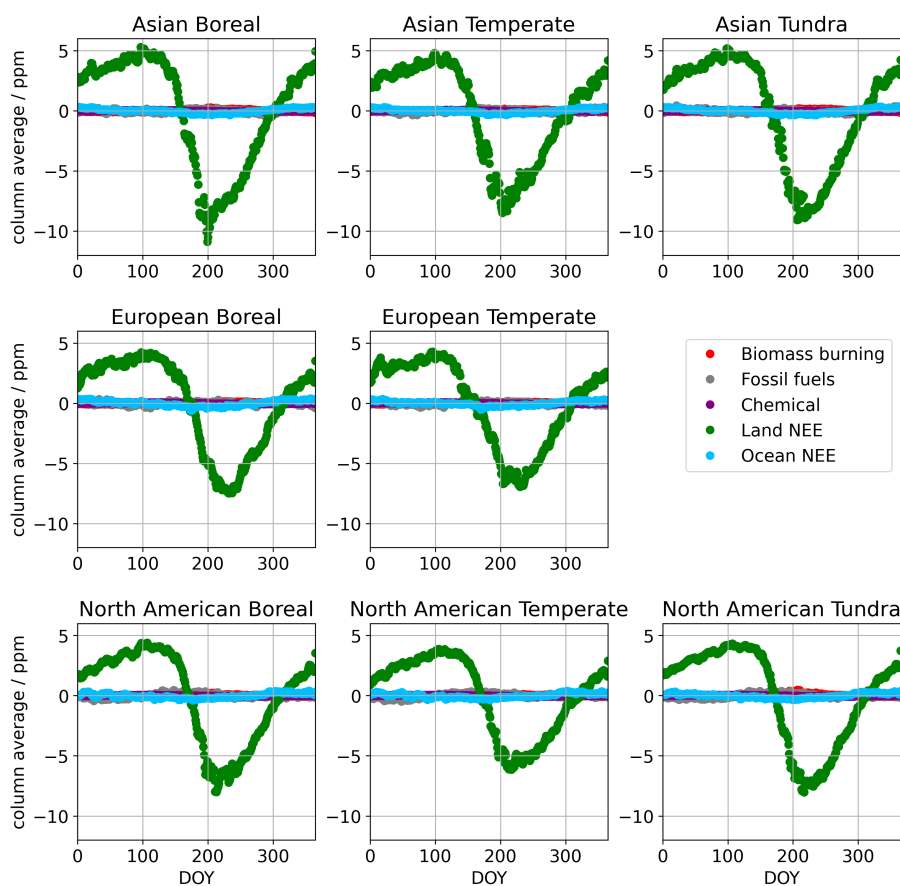


**Figure 8.** Detrended seasonal cycles of GEOS-Chem source contributions to column average CO<sub>2</sub> averaged by region and day of year.

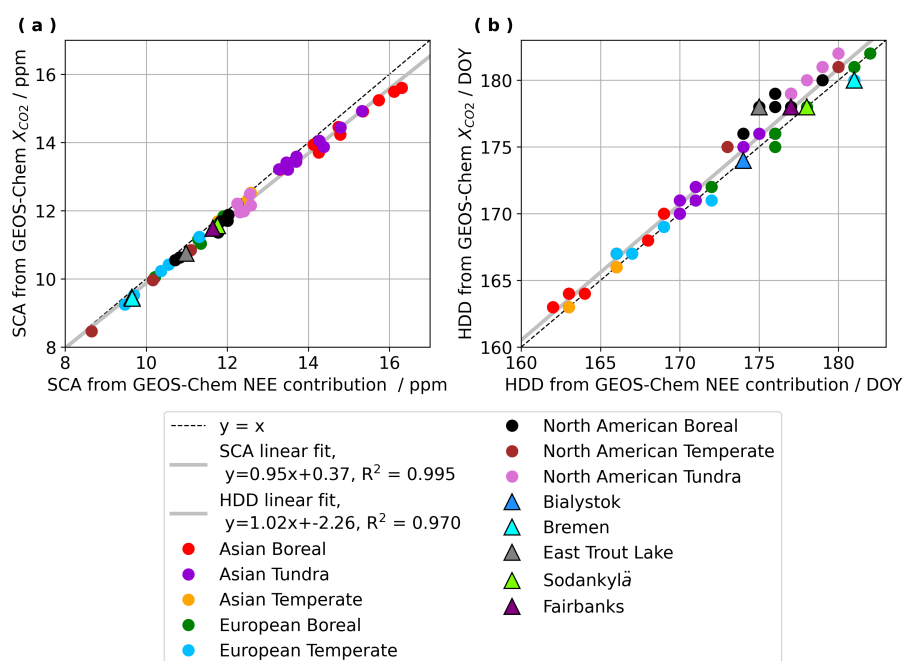


**Figure 9.** Correlations between SCA (left) and HDD (right) from GEOS-Chem  $X_{CO_2}$  seasonal cycles and GEOS-Chem source contribution of terrestrial NEE to the column.

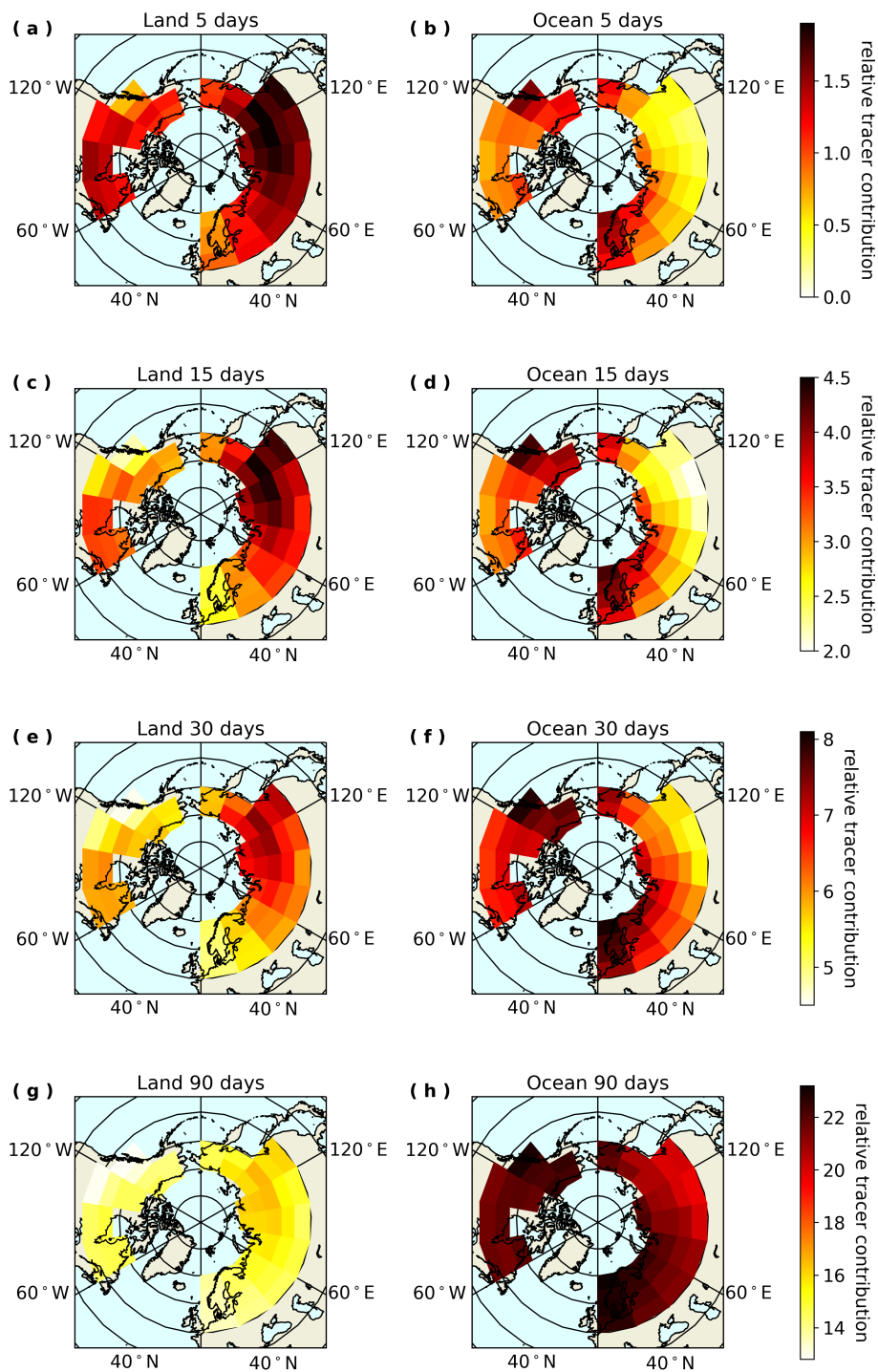


**Figure 10.** Maps of GEOS-Chem surface contact tracers on several timescales for each zone, with units that are scaled relative to an arbitrary initial release of tracer particles.

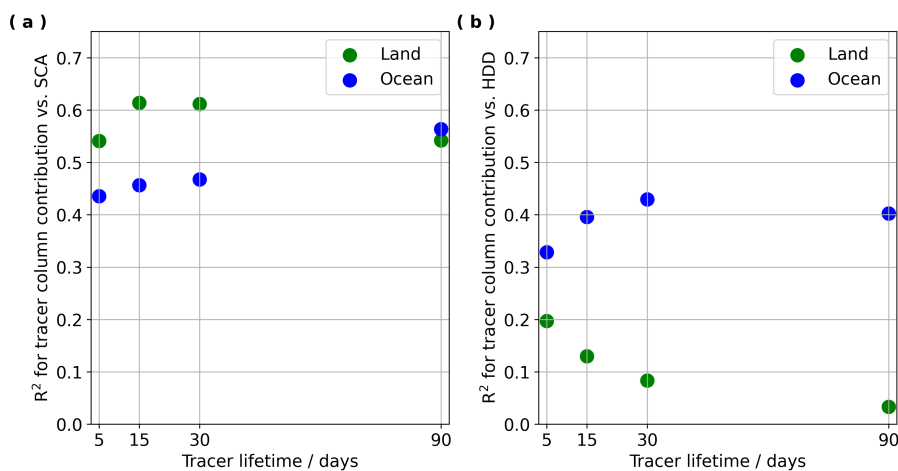


**Figure 11.** Correlation coefficients for column contributions of tracer vs. OCO-2 SCA (left) and column contributions of tracer vs. OCO-2 HDD (right).

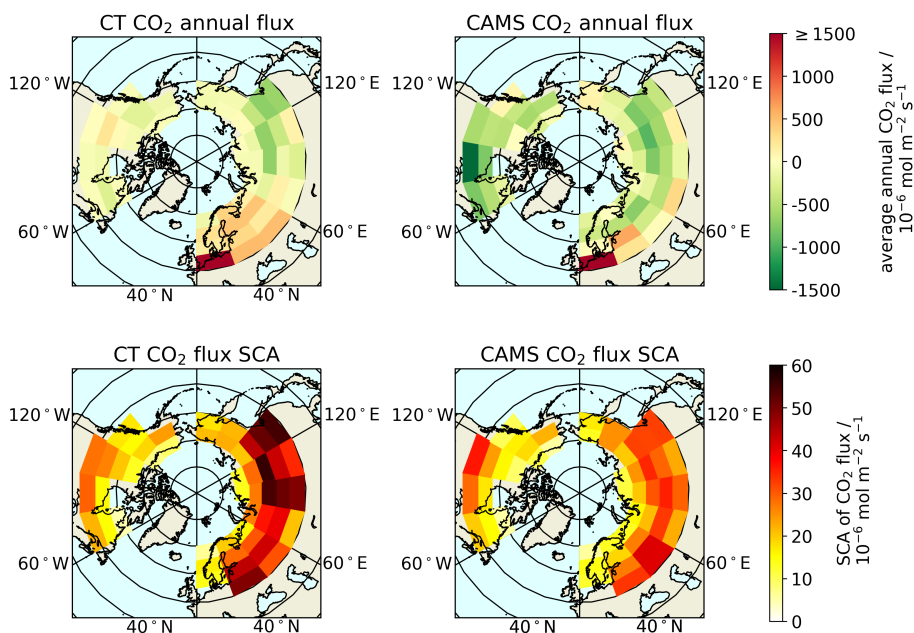


**Figure 12.** Maps of average total annual CO<sub>2</sub> flux, using GEOS-Chem (GC) and CAMS flux estimates (top), and SCA in CO<sub>2</sub> flux, calculated as the difference between the maximum and minimum of the average annual cycle in flux (bottom).



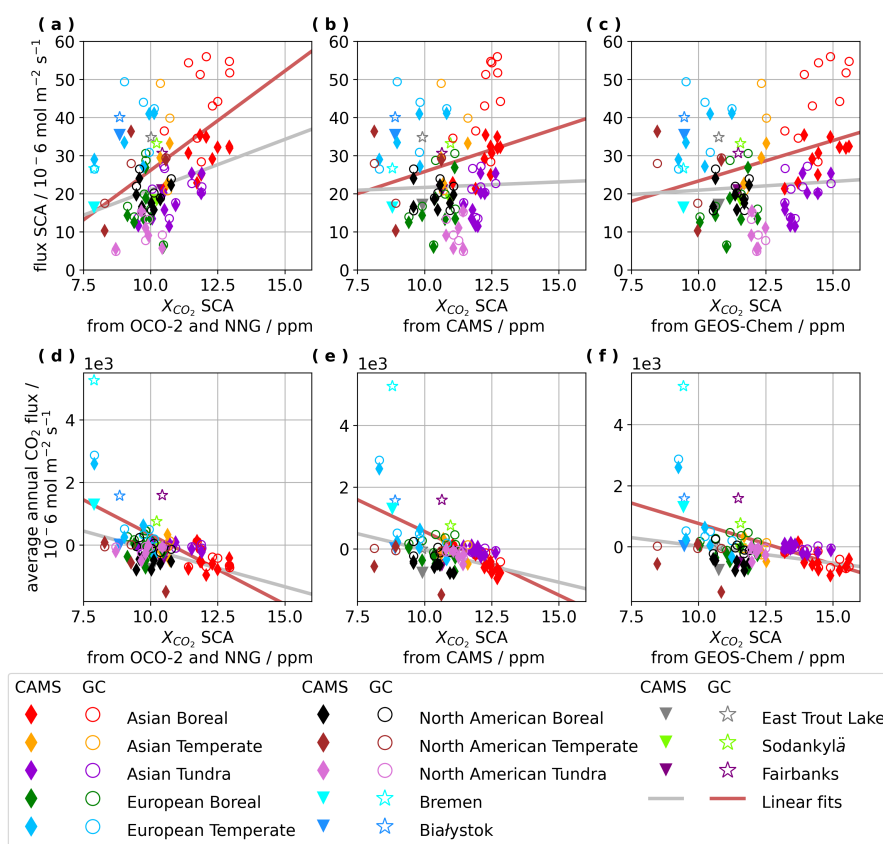


**Figure 13.** Correlation plots of flux SCA and average annual fluxes from CAMS and used in the GEOS-Chem CO<sub>2</sub> simulation against X<sub>CO<sub>2</sub></sub> SCA from OCO-2 and NNG, CAMS model estimates, and GEOS-Chem model estimates.

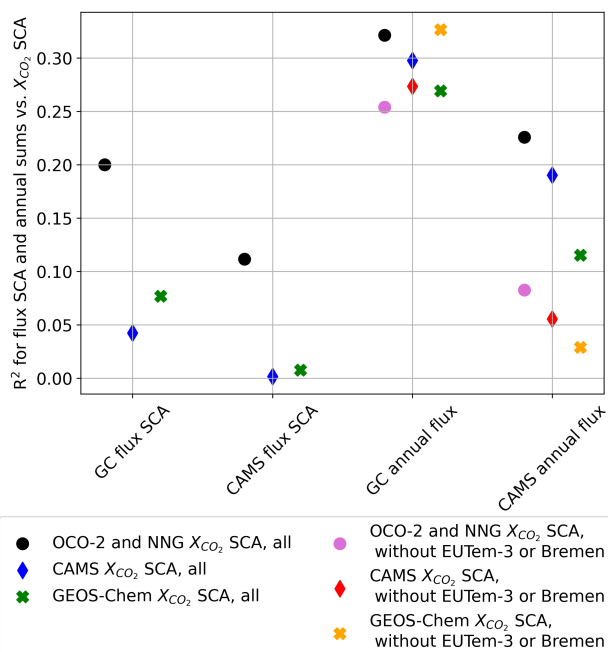


**Figure 14.** Correlation coefficients for the linear fits in Fig. 13, as well as alternative correlation coefficients for average annual fluxes vs.  $X_{CO_2}$  SCA with European Temperate zone 3 and Bremen removed.